ABSTRACT

Real-Time Modeling, Simulation and Analysis of a Grid Connected PV System with Hardware-In-Loop Protection

Feyijimi R. Adegbohun, M.S.E.C.E.

Mentor: Kwang Y. Lee, Ph.D.

Renewable energy resources have become an integral part of the power and energy industry in the world today. Photovoltaic (PV) systems are one of the most common and established forms of renewable energy technologies. With the increased installation of PV systems both on a small and large scale, it is critical that the impacts and operations of PV systems are accurately modeled, simulated and studied.

This thesis focuses on introducing a real-time simulation approach to the study of renewable energy resources that are grid connected. PV systems are the main focus of this thesis, highlighting some of the technical challenges involved in the integration of PV to the main power grid and presenting technical solutions that mitigates some of these challenges.

The real-time simulation environment presented in this thesis is the Real Time Digital Simulator (RTDS). Furthermore, the model is interfaced with protection relay testing equipment to simulate hardware-in-the-loop testing.

Real-Time Modeling, Simulation and Analysis of a Grid Connected PV System with Hardware-In-Loop Protection

by

Feyijimi R. Adegbohun, B.S.

A Thesis

Approved by the Department of Electrical and Computer Engineering

_____

Kwang Y. Lee, Ph.D., Chairperson

Submitted to the Graduate Faculty of
Baylor University in Partial Fulfillment of the
Requirements for the Degree
of

Master of Science in Electrical and Computer Engineering

Approved by the Thesis Committee

_____

Kwang Y. Lee, Ph.D., Chairperson

_____

Randall B. Jean, Ph.D.

_____

Jonathan H. Rylander, Ph.D.

Accepted by the Graduate School

May 2017

_____

J. Larry Lyon, Ph.D., Dean

Page bearing signatures is kept on file in the Graduate School.

TABLE OF CONTENTS

LIST OF FIGURES

LIST OF TABLES

ACKNOWLEDGMENTS

I would like to thank God almighty for making the completion of this thesis a reality. I would like to thank my family especially my mother Tofunmi Akamo, and my Fiancé, Taylor Winfield, for unflinching support and encouragement through my graduate school. I would like to thank my advisor Dr. Kwang Lee, for his diligent guidance and help throughout my graduate school career. I would like to thank Dr. Randall Jean, for his support and guidance throughout my graduate school and for giving me the opportunity to be part of the Baylor University graduate program and the ECE department. I would like to thank Andrew Mattei for his extremely helpful professional insight on power systems protection and Brazos Electric for donation of equipment that was instrumental to this research. I would also like to thank my good friends Noman Humayun, Adam Patino, Soumyadeep Nag, Wenlei Bai and Guiying Wu for their help and contributions that aided the completion of this thesis work in some capacity.

I would also like to thank RTDS Technologies, Ramsin Eyvaz and Juan Castaneda for their technical support while navigating through RTDS.

DEDICATION

To my mother Tofunmi Akamo, a virtuous woman who has seen me through my highest level of education with words of encouragement, thoughts of prayer and actions of endearing support.

CHAPTER ONE

Introduction

1.1 Motivation

Renewable energy resources (RER) have become a vital part of how the worlds energy needs are met. According to the International Energy Agency (IEA) renewable energy accounted for 22% of the global electricity generation in 2013 and their 2015 reports foresees those numbers to reach 26% in 2020 [1]. The rapid increase in renewable energy generation and integration is largely due to the economic and environmental benefits that this alternative form of energy poses, such as reduced dependency on natural gas and oil, fuel savings, increased reliability of electric power during outages or maintenance of traditional power supply, cost savings for owners of homes installed with RER [2]. The RER also serves as a viable and reliable solution to power needs in remote areas where power transmission is not geographically possible or economically efficient. This has led to an ever-increasing demand for extensive research in the area. PV generation systems account for over 178GW of installed capacity worldwide [1].

With increasingly high penetrations of RER generation systems, it is of uttermost concern that the RER generation systems connect to the grid without compromising the stability and reliability of the grid [3]. The distribution network of the power grid is traditionally designed to be radial; however, introduction of RER into the system, produces reversed power flow, which could be detrimental to the system. Increased installation and integration could adversely affect the grid if certain standards are not met and design is not

critically studied before implementation. The integration of RER to the grid has therefore sparked the need for developing advanced control schemes and protection techniques that meet certain standards. Some of such standards, which are the basis of this work include the IEEE std. 1547 and the IEEE std. 929-2000.

Design and implementation of RER that meet such standards requires extensive modeling, simulation and testing of the system. Specifically for PV systems, accurate simulation, modeling and testing is required to study the impact of the PV systems on the grid and vice versa. It is also important to test and study protection of both the PV system and the grid during contingency situations.

The scope of standards such as the IEEE std. 929-2000 are simply a guide of recommended practices that describe specific recommendations for "small" systems, rated at 10kW or less. This depicts smaller PV systems that may be used in residential areas or organizations such as schools, hospitals, manufacturing companies, etc. However intermediate PV systems from 10kW to 500kW can follow similar guidelines and recommendations [4].

The standards mentioned above provide guidelines for studying technical issues affecting PV integration with the main grid such as [4][5], Island operation of PV system, Anti-Islanding/Non-Islanding scheme, Power Quality, Power system topology of PV system, Structure of PV systems & Control Requirements, and Safety & Protection.

In order to meet the critical standard requirements for design of a PV system , a robust simulation and testing environment is required. Models that meet the requirements must be developed in such an environment and such models must be simulated and tested to attest to the viability of the system according to the standard. The proposed simulation

environment for this work is a real-time simulation environment, specifically, RTDS. Real-time simulators have a vast number of advantages in power system simulation, for example real-time simulation allows for the simulation/testing of the system for real scenarios that cannot ordinariliy be carried out on the real system, such as an outage or a contingency situation, thereby providing accurate data of how such situations should be handled in case such an event occured in the real world. Additionally, real-time simulation provides time saving advantages in the case of simulating longer periods of simulation data such as a daylong load forecast, wind forecast, or temperature forecast. Most importantly, real-time simulators are equipped with the ability to interface real hardware to the simulated model such as protection hardware (Relays, PMU), power hardware (Solar Panels) or control hardware, making hardware-in-the-loop simulation possible.

1.2 Research Objective

Real-time simulation of power systems is a fairly new technology used in the area of power and energy; however, it is applications are extremely vast and powerful. The main objective of this research is to develop a detailed real-time model of a PV generation system integrated with the grid and to implement real-time control and protection techniques with real protection hardware interfaced with the model.

The research objectives to fulfill the requirements of this thesis are listed as follows:

- Literature review of grid connected PV generation system identifying technical challenges faced by the technology.
- Literature review of Real-Time Digital Simulator (RTDS) and development of real-time RER generation system model in RTDS.
- Detailed development of grid connected PV generation system model in RTDS.

- Interface of grid connected PV generation model with real protection hardware.
- Transient/Steady State analysis of PV system connected to grid.

1.3 Thesis Organization

The first chapter of this thesis gives a general overview of RER, Real-time simulation and motivation for this research.

Chapter Two identifies previous work that has been done in this area of research, reviewing the literature that identifies some of the technical challenges that lead up to the studies covered in this research.

Chapter Three extensively discusses the RTDS and its various capabilities, this chapter is aimed at helping readers of this thesis become more familiar with real-time simulation environments

Chapter Four discusses the development and modeling of the PV systems connected to the grid. Identifying different control strategies implemented in achieving reliability and stability of the system. The analysis of the PV system designed is also covered in Chapter Four as the performance of the systems controls and power quality is analyzed in relation to specified standards.

Chapter Five describes the implementation of interfacing protection equipment to demonstrate hardware-in-loop (HIL) testing. The various scenarios and test cases implemented in the simulation are presented and thorough analysis of the system's transient response is given in relation to specified standards in order to illustrates the viability of the designed system.

Chapter Five also presents results of simulation test cases carried out to verify the implementation of HIL system protection according to IEEE PV to grid interface standards.

Chapter Six provides the conclusion of the thesis and highlights future research work in this area.

CHAPTER TWO

Background and Literature review

2.1 Introduction

Over the past decade, Renewable Energy Resources have become more popular and is considered to be the future of energy globally. This has led to scholarly devoted research pertinent to the technical challenges surrounding the technology, popularly known as SMARTGRID. These challenges are vast, varying from modeling, developing of intelligent controls, designing of protection schemes that improve stability and reliability of the grid, simulation of power systems/grids, optimization of power flow, stochastic modeling & forecasting, synchronization of RER systems to grid, power management, cost modeling, smart energy storage systems and a host of others.

The scope of this research can be summarized to two major challenges, firstly, analyzing a real-time modeling and simulation environment. Secondly, developing a real-time grid connected RER system, specifically a PV system model, designing control schemes and protection protocols, analyzing the system and presenting results that are consistent with standard guidelines as defined in Chapter One.

This chapter provides concise definition of RER, PV Systems and Real-time Simulation. This chapter also provides a technical literature review on design and implementation of a grid connected PV system, defining different concepts that allow for the implementation of PV systems today and highlights the current technical challenges faced. This chapter also serves as an introduction to the real-time digital simulator RTDS.

2.2 Renewable Energy Resources (RER) and SMARTGRID

Renewable energy resource is simply energy generated from a natural resource, such as sunlight, wind, rain, tides, and geothermal heat, that can be renewed or replaced naturally (unforced). Renewable energy technologies, otherwise described as RER systems, are applications of RER resources such as solar power, wind power, hydroelectric power, bio fuels and so on.

The term SMARTGRID varies in meaning, fundamentally it refers to important issues surrounding the integration of RER and the future of the power grid as it continues to evolve. The modernized grid or SMARTGRID offers real time information on the grid's status such as amount of backup generation in operation, generation available, peak load information, offline and online generation through advanced communication and metering technologies, and real-time control through technologies such as SCADA. The SMARTGRID is also considered to be self-reliant (autonomous) and capable of handling high penetration of renewable energy resources.

2.3 Photovoltaic (PV) System

Solar energy is the most available form of energy and is also one the most common forms of RER used globally [6]. Photovoltaic systems are systems that convert solar energy into electrical energy that are typically either stored locally, support a local load, or fed back to the main power grid. Implementation of PV systems have many advantages and are made possible through SMARTGRID applications; however, PV systems face various technical challenges such as variation in performance due to variation in weather, high installation and implementation costs, and low efficiency [6]. In order to meet some of the

various challenges that PV system implementation faces, advanced controls must be developed.

2.4 Overview of PV System Control

PV systems have different characteristics that are non-linear [7] such as being constantly affected by a constant change in temperature and weather. In order to increase efficiency of PV system and maintain stability of the system without compromising the stability of the grid, several advanced control strategies have been implemented. Some of such control strategies are highlighted in this section

2.4.1 MPPT Control

Maximum Power Point Tracking (MPPT) is an important control strategy that is critical to both the efficiency and power control of the grid connected PV system. Extensive work has been done thus far in MPPT control. [8] Presents Particle swarm optimization (PSO) applications in MPPT, in [7] a proposed neural network algorithm for MPPT control is presented. Other traditional and modifications to traditional methods such as incremental Conductance Method, which is based upon the Hill Climbing Method or otherwise known as the Perturbation & Observation Method is adequately discussed in [11] – [12].

The method implemented in this thesis is Incremental Conductance Method, which is an augmented form of the PO method [8]. The details of this method will be further discussed in the following sections.

2.4.2 Voltage Source Inverter

Connecting non-dispatchable forms of energy or RER such as PV to the grid involves the use of power electronic inverters. Therefore, the topology of such inverters

for the DC/AC conversion of PV output voltage is an area critical to the operability of PV systems that are grid connected. This area has also been widely studied with various forms of topologies and types of power electronic switching devices proposed. These switching devices call for higher voltage, low-frequency switching insulated gate bipolar transistor (IGBT), and lower voltage, high-switching frequency metal oxide semiconductor field effect transistor (MOSFET) [13]. Reference [14] presents the topology of Voltage Source Inverter proposed in this thesis. Reference [15] Provides an in-depth study of different converter topologies and their various applications. In [16], explanations of the concept of power electronic converters, basic configuration of Voltage Source Converter (VSC), modeling of VSC and control of VSC are presented. The topology of power electronic inverters otherwise reffered to as VSC implemented in this work stems from [16]. Sinusoidal pulse width modulation SPWM is implemented in the control of the switches in the VSC.

2.4.3 Power Control of PV System

The power control of the PV system is essential to continuously keeping the PV system in synchronization with the main grid, while maximizing power output. In [17] a grid-connected PV system is modeled and simulated in PSCAD software. A decoupled current control strategy is used to control the real and reactive power injected into the grid. The power controller serves as an upper level controller, regulating q-axis and d-axis current orders. These produce current references which serve as inputs to the current controller [17]. The decoupled current control outputs are modulation signals that control SPWM firing pulses of the voltage source converter.

2.4.4 PV System Protection

The variable and non-dispatchable nature of PV systems makes protection of PV systems increasingly difficult. In [18], [19] protection schemes for stand-alone PV systems and Offshore Island with High PV penetration are discussed. In [20], [21] Anti-Islanding protection schemes are presented for grid connected PV systems applications. In this work protection schemes for Over/Under voltage, Over/Under frequency, Over/Under Current are implemented in a real-time environment.

2.5 Summary

In this chapter a brief overview of the literature that covers previous work done by researchers in the area of RER, particularly for PV system integration to the grid is presented. However, simulations and studies are performed on a purely software simulation platform and not a real-time environment such as the RTDS. The main objectives of this research as stated in Chapter One is to implement PV system in a Real-time simulation environment, presenting accurate results that can be implemented in the real world. The following chapter discusses in great detail the RTDS whish is used to achieve this objective. Identifying all of the key functions and capabilities of the Simulator, its various applications and providing a step by step guide on how a power system model can be fully developed and simulated.

CHAPTER THREE

Real Time Simulation

3.1 Introduction

Power systems modeled and designed for real world applications should be accurately tested for viability and reliability. Control and protection devices for power systems should also be tested adequately in order to verify their compatibility and effectiveness before they are installed into the system. More importantly power systems should be tested for various scenarios that could pose a grave risk to the grid. Real-time simulators have several advantages; allowing operators to simulate contingency or test procedures that cannot be readily simulated on the real system for either training or precautionary purposes. Real-time simulators also save valuable time as it relates to simulations that involve bulky data, such as hours of load forecasts, weather forecasts and so on. In addition, real-time simulators allow for hardware-in-the-loop testing of real equipment such as prototypes, protection hardware, power hardware and control devices. An ElectroMagnetic Transient Program (EMTP) based real-time simulator manufactured by RTDS Technologies is introduced in this chapter, highlighting some of its capabilities and applications.

3.2 Real-Time Digital Simulator

The RTDS uses a nodal analysis-based solution algorithm for the electromagnetic transient simulation of power systems. The concepts behind the implementation of this algorithm, which is a widely accepted by industry standard for power system simulation

programs can be found in [23]. The RTDS was developed as a result of research done by the Manitoba HVDC Research Centre in the 1980s by dedicated power globe professionals and scholars [23].

The RTDS has a variety of applications namely HVDC and Flexible Alternating Current Transmission Systems (FACT) Simulations, Protection HIL testing, Control System HIL testing, PMU Studies, Power Electronics Simulation and testing, Power HIL Simulation & Testing, SMARTGRID & Distributed Generation applications such as Supervisory Control and Data Acquisition (SCADA), as well as serving as an Education/Training tool [23].

EMTP power network solutions are based on the dommel algorithm which converts the network into a norton equivalent circuit. In real-time digital simulations, network solutions are calculated at every time for network voltages and currents, usually at 50μs for a 60Hz system, therefore operating at a sampling rate of 20kHz and being amply sample all of the transient operations of the power network at a very high resolution. Controller actions are computed and are triggered in real time at every instance and the network solution is recalculated at the next time step. In the case of power electronic converters, smaller time steps must be achieved to accurately simulate the switching speeds of the power electronic converters. 1-3μs are the requirements for representation of converter switching speeds [25].

The RTDS consists of hardware and Software tools that combine to form a completely real-time simulation environment that is tailored to simulation of power systems. The design and development of the power system and controls are carried out in the RTDS software, RSCAD, which also serves as a Graphical User Interface (GUI) for

monitoring the system during runtime. The computations, communication and HIL interface is performed by the RTDS hardware.

3.2.1 RTDS Hardware

The RTDS hardware features a cubicle that hosts powerful processor cards (GPC/PB5), capable of computing the entire network solution in real time, as well solving auxiliary components such as transmission line parameters, generators, etc. The processor cards also compute controls of the systems as well, also in real time. In addition, each card includes d/a analogue output channels ranging from +/- 10 *Vpeak* that can be connected to an oscilloscope and used to measure out signals in real time [25].

Every RTDS hardware is also equipped with a Giga Transceiver Workstation Interface (GTWIF/WIF) card. The GTWIF card serves solely as communication between the RTDS software, RSCAD, running on the computer workstation and the host of hardware components on the RTDS rack [25]. The communication is done over ethernet based Local Area Network (LAN).

In addition to the processor and communication cards, the RTDS is also equipped with a host of other add on cards, which make several of the aforementioned HIL simulation possible. The Giga Transceiver Network (GTNET) card can be used to interface several standard network protocols such as [25]:

- GSE/Goose IEC-61850 standard
- SV IEC-61850-9-2 (sampled values)
- DNP3 Distributed Network Protocol
- PLAYBACK playback of large data sets

The Gigabit Transceiver Analogue Output (GTAO) card can be used to interface analogue signals from the RTDS system to external devices. The GTAO card includes twelve, 16-bit analogue output channels with output range of +/-10 volts [25]. Chapter Five presents an application of this card and provides further details on its capabilities.

The Gigabit Transceiver Analogue Input (GTAI) card is used for analogue interface of input signals from external devices to the RTDS, The Gigabit Transceiver Digital Input card (GTDI) is used to interface digital signals from RTDS to external equipment, and the GTDI is used to interface digital signals from an external device to the RTDS.

The Giga Tranceiver Front Panel Input (GTFPI) card forms an interface between the digital I/O panel and the GT port of on the GPC card. The GTFPI acts as a direct digital interface to the GPC card, and can be used as a means to directly send control input signals to the RSCAD model during runtime.

Figure 3.1 shows the actual hardware set up of the RTDS in the Power & Energy Systems Lab at Baylor University. Mounted on the rack are two GPC cards, a GTWIF card, GTFPI, and an SEL-421 Protective relay for HIL simulation and testing. The relay is connected physically to the RTDS through GTAO card (not shown).

3.2.2 RTDS Software – RSCAD

The software counterpart of the RTDS real-time simulation environment, is one aimed at providing a familiar user interface for power system engineers to develop and test power systems [23]. It is packaged software that provides users with all the necessary tools to develop a complete power system model, including a wide range of the power system components, control system tools and power system protection modules.

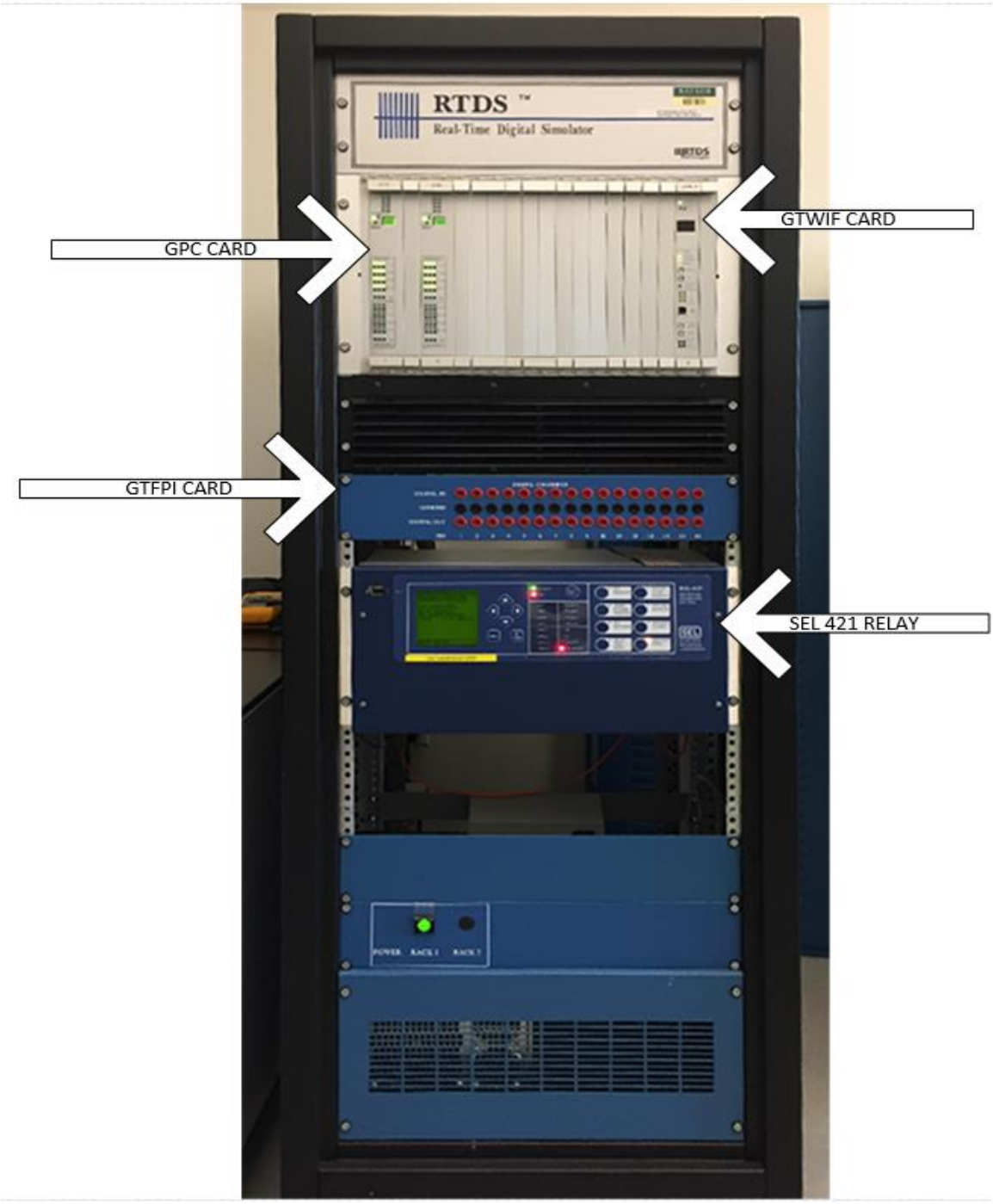

Figure 3.1. RTDS Setup in Power & Energy Systems Lab.

The software also doubles as a graphical user interface for monitoring the system operations in real time, and provides abilities to adjust system parameters in real time.

The RSCAD software is further divided into several different modules, the different modules that exist in software are shown in the File Manager in Figure 3.2 below, however the most commonly used modules are DRAFT, RUNTIME, CBUILDER and T-LINE.

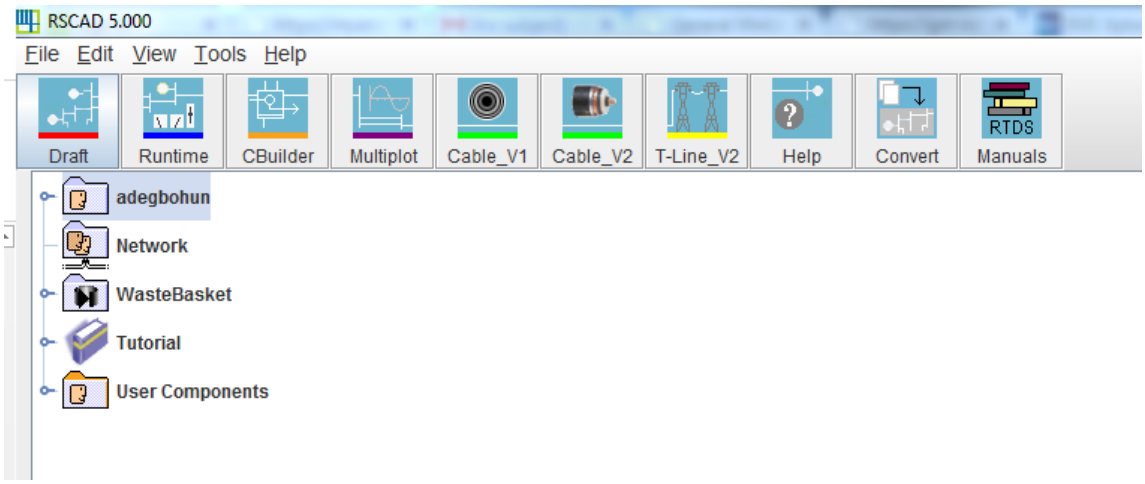

Figure 3.2. RSCAD File Manager.

RSCAD DRAFT

The RSCAD draft is a graphical user interface where the user can assemble a schematic diagram of system using components available in the RSCAD component libraries. A model can be assembled on a blank draft template file by selecting the draft and choosing "New Circuit", this creates a new draft file. Sample models and tutorial models are also available in the File explorer that can be modified to suite the users' objectives.

Models/Schematics can be built in single-phase or three-phase according to the users specified preference. Both three-phase and single-phase components are also generally available in the library except otherwise specified.

Components library in the DRAFT is further sub divided into different categories, The power systems library contains power system components such as buses, wires, loads, branch components made up of R's, L's & C's and so on. The power system library also contains power system models such as source models, fault & breaker models, transformer models, instrument transformer models, machine models, SVC models, etc.

The controls library contains novel control models such as math functions, logic functions, transfer functions, signal generators, meters, signal selectors, signal processing models and so on. The controls library also contains I/O components that are unique to the RTDS. These components represent a graphical representation of the physical hardware used for HIL simulation in RTDS.

In order to simulate power electronic switching dynamics, a smaller time step solution is required [25]. The RSCAD DRAFT makes provision for small time step components in the small-time step library which features VSC branches, different VSC models and topologies, VSC interface transformer models and other small time step components.

Other component libraries found in the RSCAD DRAFT include generator control libraries, which consists of IEEE standard generator exciter models and Protection and Automation libraries which consists or standard relay models for generator protection, distance protection, overcurrent protection, differential protection, breaker control models and so on. The Automation libraries also include graphical representations of communication and network interface cards that can be used for standard network protocols such as DNP, GSE/Goose, SCADA, SV1 and so on.

Figure 3.3 is a representation of a draft case in RSCAD. On the left-hand side, we have the draft template and on the right-hand side we have the components libraries as described above. After a draft schematic has been created, the compile button can clicked in the toolbar above the template, the compiler software essentially converts the graphical representation of a power system designed in the draft into machine level code which is executed during run time [25].

RSCAD RUNTIME

The RSCAD RUNTIME is a graphical user interface representation of the machine level code generated when the user compiles a draft case. In the RUNTIME, the user can measure and preselected signals from the runtime in various forms such as plots, meters, timing charts and so on. The user can also manually control parameters in real time using inputs such as push buttons, sliders, dials, switches, etc. As inputs are made to the real-time system, the measurements are updated immediately and monitored signals reflect these changes. The RUNTIME environment also has a unique feature which allows the user the record a series on manually controlled inputs and generates a SCRIPT file which can be played back into the RTDS in runtime. The function of a script file is to control the operation of the simulator, collect and analyze data without direct user interaction.

Figure 3.4 is a representation of a RSCAD case during RUNTIME illustrating some of the different features mentioned above. During runtime, it is possible to adjust different parameters of the system using manual inputs such as switches, dials, sliders and push buttons. While applying such inputs, we can also observe the response of the system in real time through the updated plots.

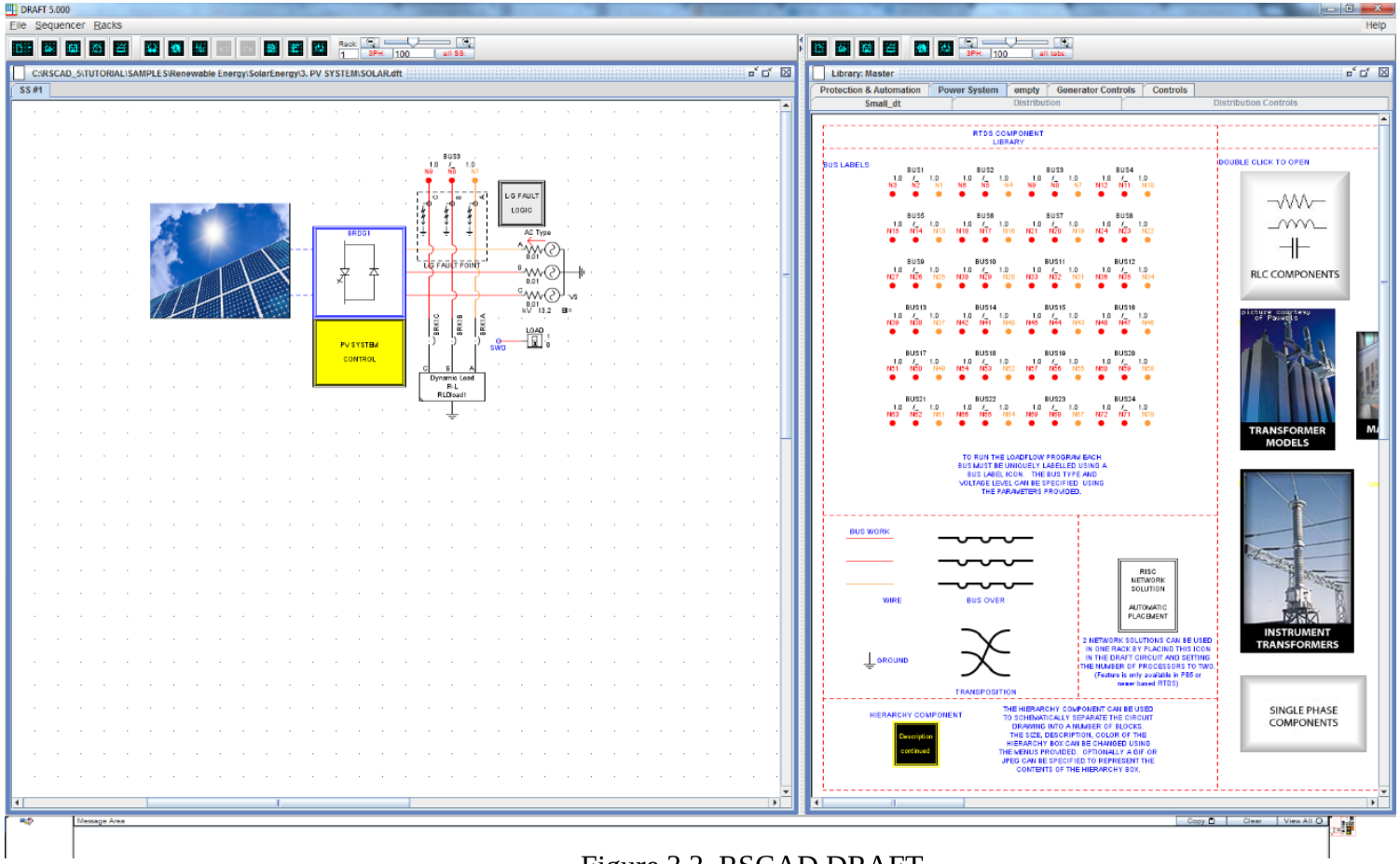

Figure 3.3. RSCAD DRAFT .

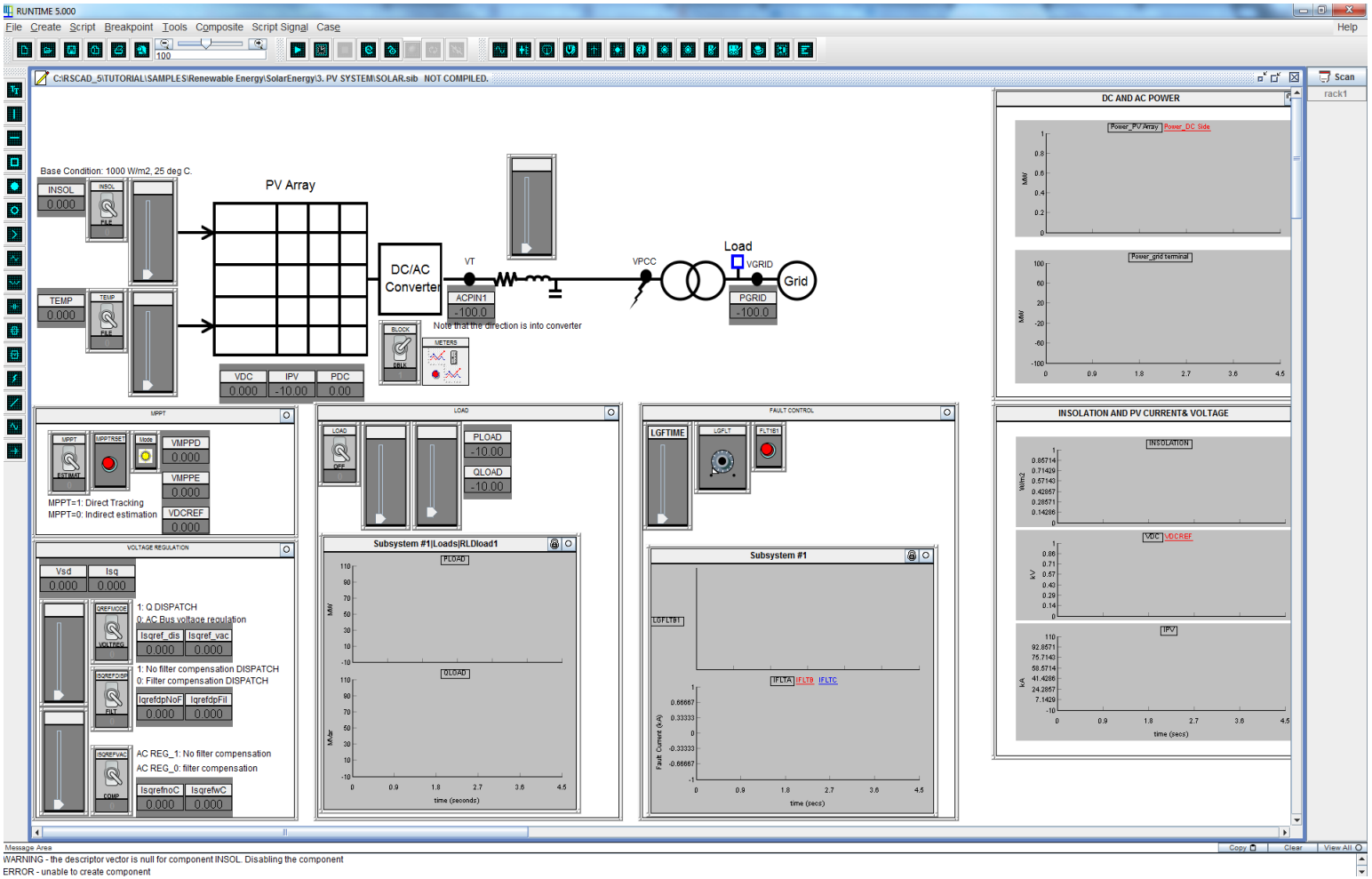

Figure 3.4. RSCAD RUNTIME.

3.3 Summary

This chapter provides an overview of RTDS Technologies real time digital power system simulation environment. It highlights some of its major capabilities and applications and provides a detailed guide on getting started with the RTDS and RSCAD software.

CHAPTER FOUR

Real Time Modeling and Simulation of Grid Connected PV Generation System

4.1 Introduction

This chapter presents a real-time approach to the development of a grid-connected PV generation system model. In a grid-connected PV generation system, the available power supplied to the grid side is determined by solar irradiance and temperature. Interaction of the PV generation system with the grid is based on power electronic converter topology and control. The different sections in this chapter cover the complete design implementation of the system and extensive analysis of the entire systems operations and controls in real time.

4.2 PV System Configuration

Figure 4.1 provides conceptual details of the topology of the circuit that will be constructed in the RTDS. The system is a grid connected PV system [26] consisting of a PV array, dc-link capacitor, single stage voltage source converter, harmonic filter (LC type) , a grid interfacing transformer and infinite bus representing the grid side.

The circuit configuration in the RTDS differs slightly from a practical PV generation system; however, the operation of the system matches accurately with practical system due to real-time approach to modeling and design of the various components of the PV system.

The grid-connected PV generation system constructed in the RSCAD software of the RTDS is shown Figure 4.2. Detailed descriptions of each of the major components and the PV control system will be discussed in the following sections.

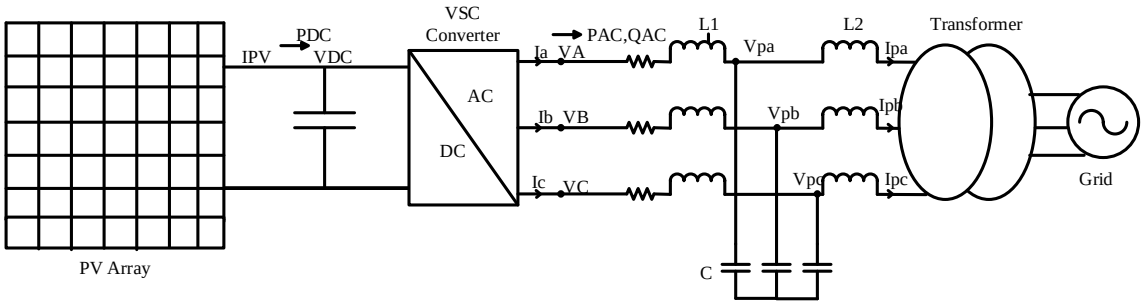

Figure 4.1. PV System Configuration.

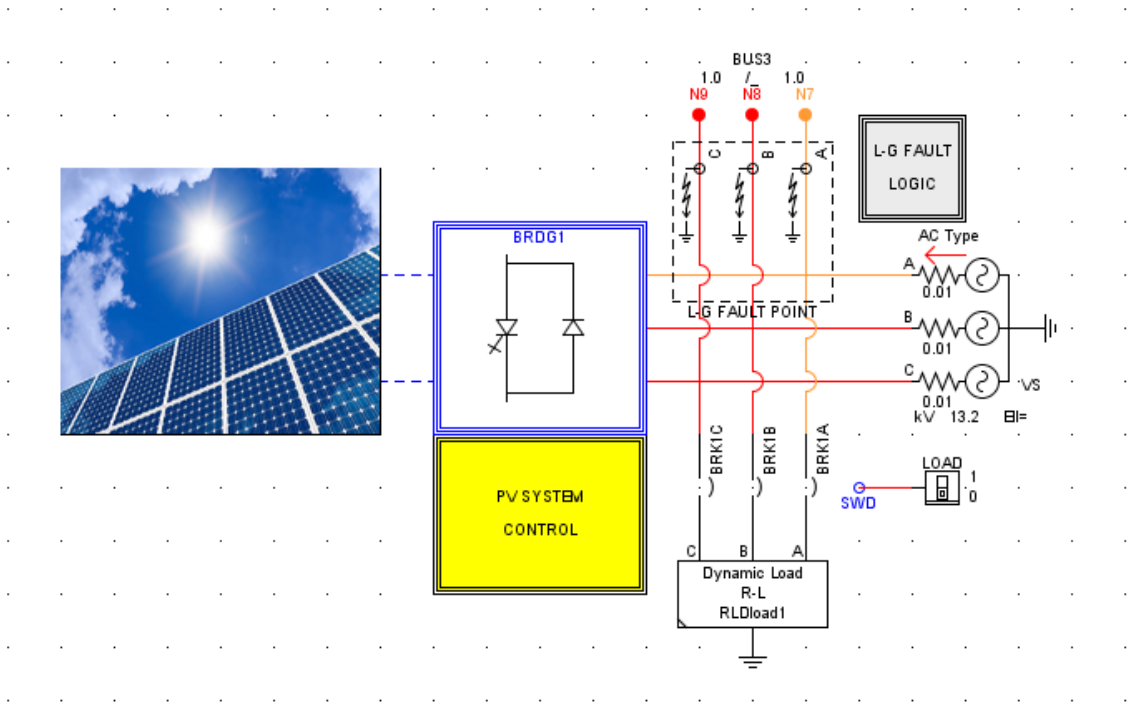

Figure 4.2. PV system constructed in RSCAD.

The PV System ratings and parameters are listed in Table 4.1.

Table 4.1: PV System Parameters [26]

Variables	Values
Rated PV Power	1.74MW
Rated DC Voltage	2kV
LV Transformer winding	0.48kV
Transformer leakage reactance	0.15pu
Transformer rating	2.5MVA
Grid Frequency	60Hz
Interface reactance	100mH
Resistance of Interface reactor R	2mΩ
Dynamic Load	1MW, 0.1MVat Initial

4.3 RTDS PV Array Circuit

Figure 4.3 represents the RSCAD model of a PV array in RTDS. The PV arrays consists of solar cells made of semiconductor materials such silicon, germanium, etc. Semiconductor materials have the capability of producing electrical charge when exposed to direct sunlight. In most cases, numerous cells are connected in series to form what is called a PV module. The PV modules are further combined in both series and parallel to form what is known as a PV array. Figure 4.4 gives a description of PV cell, module and array.

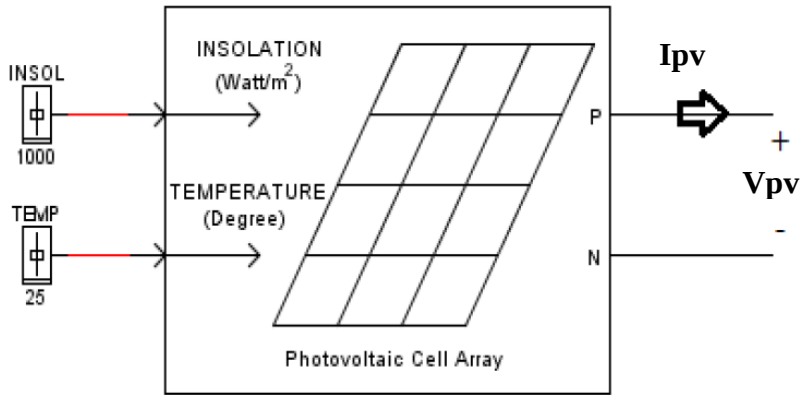

Figure 4.3. RTDS PV Array Model [25].

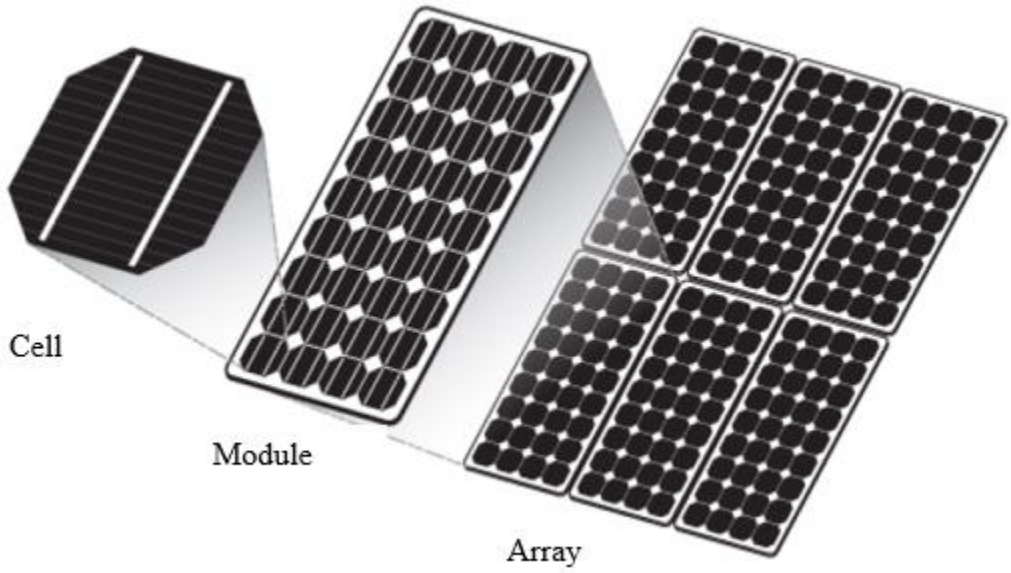

Figure 4.4. PV Array, cell, module description [6].

For practical purposes, the PV cell is electrically represented as a current source in parallel with a single diode shunt resistance and with a series resistance as shown in the Figure 4.5 below.

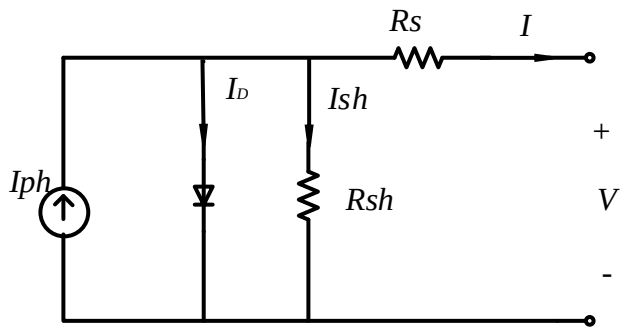

Figure 4.5. Practical Model of a PV Cell.

A current-voltage relationship of the PV cell model is defined by equations (4.1) and (4.2) below:

$$I = I_{ph} - I_D - I_{sh} \tag{4.1}$$

$$I = I_{ph} - I_o(\exp\left(\frac{V + R_s I}{N_c a V_t}\right) - 1) - \left(\frac{V + R_s I}{R_{sh}}\right) \tag{4.2}$$

The photocurrent *Iph* is the current induced by the incidence of sunlight on the solar cell. The diode current I_D produces the I-V characteristic of the PV cell where *Io* is the diode reverse saturation current. The diode ideality factor *a* is a measure of how closely the diode matches the ideal diode equation. The series resistance *Rs* is the sum of several structural resistances in the solar cell while the shunt resistance *Rsh* represents the leakage current of the semiconductor material and the manufacturing process of the solar cell [27, 28], and V_t is the diode thermal voltage which is a constant defined at any given temperature *T* (in K) by [27, 28]:

$$V_t = \frac{kT}{q} \tag{4.3}$$

where *k* is the Boltzmann constant (1.3806503x10-23J/K) and *q* is the magnitude of an electron charge (1.602176x10-19 C).

The relationship between the current and voltage of a PV cell is shown in Figure 4.6. The relationship ranges from the short circuit current (0, *Isc*) to open circuit voltage (*Voc,* 0) with a knee point (Vmp, Imp) defined as the maximum power point where the PV array generates maximum electrical power *Pmax*.

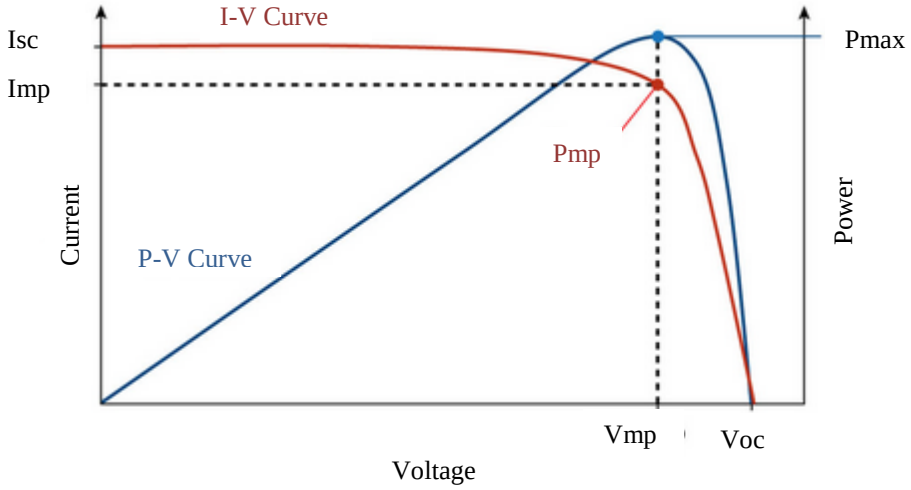

Figure 4.6. I-V and P-V curve of a PV array system [25].

The I-V characteristics of solar depends on the semiconductor material as well as variation of solar parameters such as the solar intensity *G* and temperature *T*. Reference solar irradiance/intensity is usually set to 1000W/m^2 and temperature at 25^{0}C. Table 4.2 summarizes the PV parameters and data used in this particular simulation.

The PV array system simulated in this word features a combination of 115 series modules and 285 parallel modules in total to form a PV system rated for 2kV and 1.74MW.

Table 4.2: PV Array Parameters.

Unit	Parameter	Value
PV Module data	Temperature ref	298K / 25^0C
	Irradiance ref	1000W/m^2
	Open-circuit voltage at ref	21.7V
	Short circuit current at ref	3.35A
	Max power at ref	1.74MW
	Voltage at max power	17.4V
	Current at max power	3.05A
	Temperature coefficient at short circuit current	0.065%/^{0}C
PV Array	Modules in series	115
	Modules in parallel	285

The PV array system as modeled in the RSCAD draft of the RTDS is shown in Figure 4.7 for the grid-connected PV system.

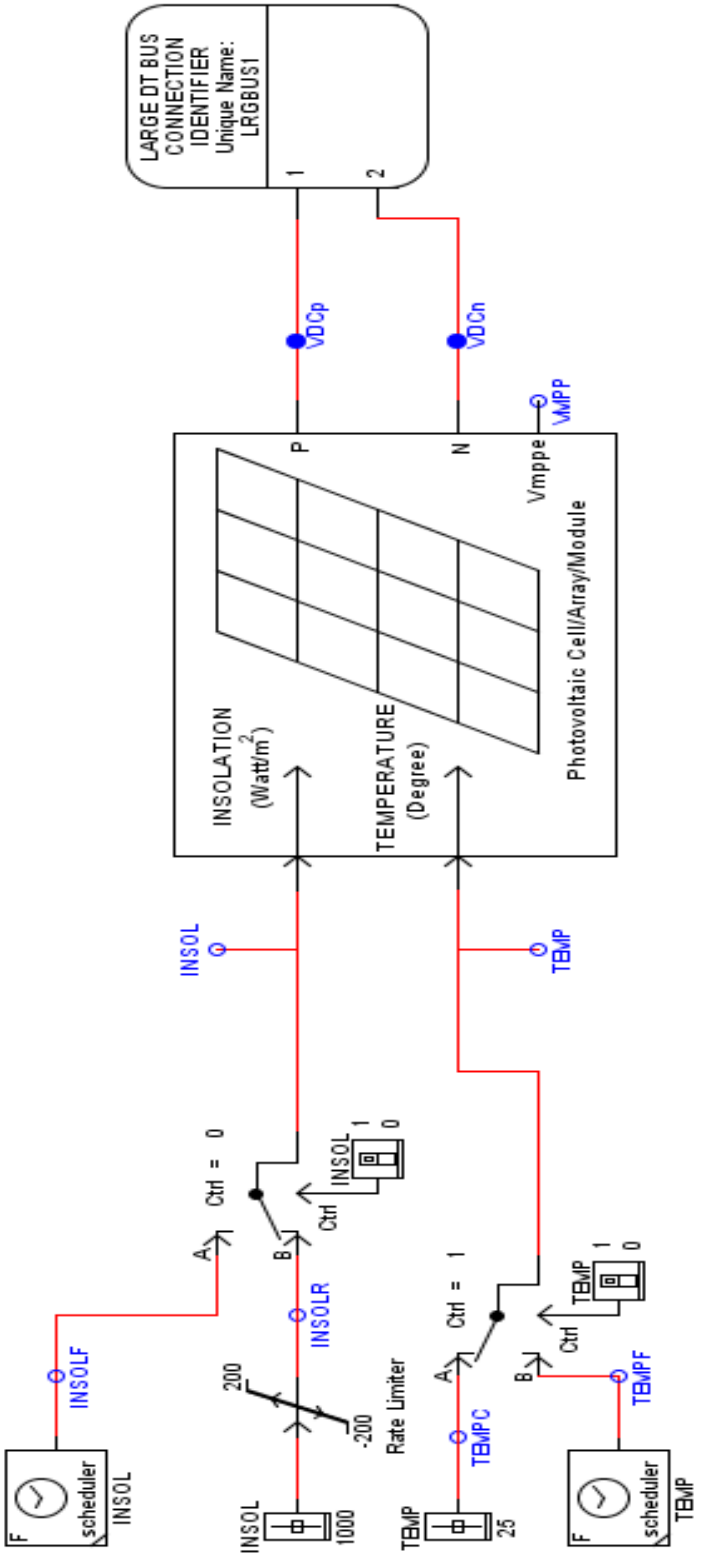

Figure 4.7. PV Array for Grid-Connected PV in RSCAD [25].

4.4 Real-Time Modeling of Grid Interfacing Inverter (VSC)

4.4.1 Background

Voltage source converters (VSC), in an electromagnetic transient (EMT) simulation program requires the representation of many closely-coupled switching devices having firing resolutions for turn-on and turn-off at high frequencies, much higher than the grid operating frequencies. Due to the speed of the switching (1.5 - 4.0kHz), typical EMTP simulation time steps of 50 microseconds are insufficient. General approaches to switching power electronic devices in an EMTP simulation network are generally accomplished by modifying the Dommel Algorithm. That is by inverting and decomposing the conductance matrix so that the voltages can be calculated. This approaches, however, are impractical in real-time simulation simply because there can be multiple decompositions of matrix required in a single time-step as a result of changes to the conductance matrix. This can be caused by the number of switches or PWM rate.

The RTDS solution approach to simulating the switching on and off of power electronic switches is called the “Small time-step”. The solution is still based on the Dommel Algorithm; however, fundamentally the Dommel Conductance matrix is never changed, irrespective of the state of the switching device. This implies that the matrix does not need to be further inverted or decomposed again to calculate the solution; however, in order to implement this algorithm certain conditions have to be met and certain assumptions need to be made.

Firstly, a switch can fundamentally be modeled as a conductance, which is extremely small when open and large when closed. Instead of modeling an open circuit (open switch) as a small conductance, it can be modeled as a series resistor R and capacitor

C; conversely, instead of modeling a short circuit (closed switch) as a large conductance, it can be modeled as an inductor L as described in Figure 4.8 [25].

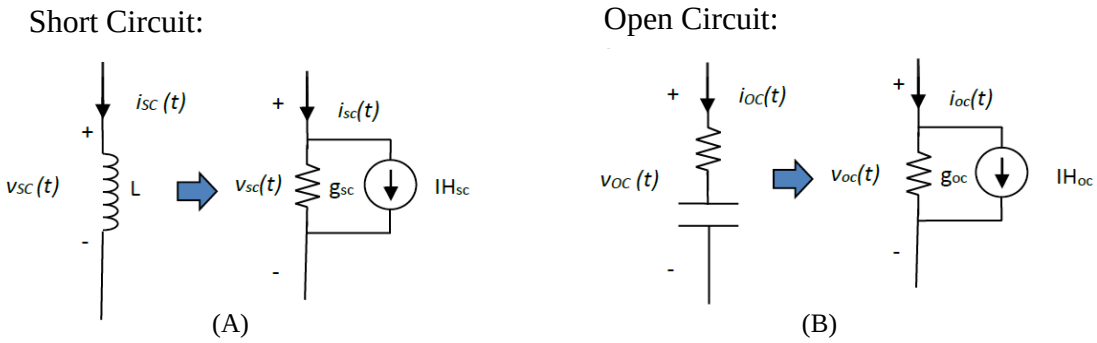

Figure 4.8. Equivalent circuits used to represent (A) Short Circuit and (B) Open Circuit in the small-time step simulation [30].

When a switch is in the "ON" state, it is thus modeled as an inductor in the Dommel Algorithm. When it is in the "OFF" state it is represented by the RC branch. The R is also picked so that if an "ON" branch is in series with an "OFF" branch, it represents an RLC circuit with a damping factor of δ. The values of R and C are selected so that together they represent a fairly large impedance across the system bandwidth and L, so it represents a fairly small impedance. These parameters, R, L and C are also selected so that equivalent conductance g_{oc} and g_{sc} are kept equal, this results in the conductance matrix remain constant for any combinations of switching, therefore the solution become trivial [25].

where selection of R, L & C are given by:

$$L = \frac{\sqrt{2}(\Delta T \bullet F)v}{i} \tag{4.4}$$

$$C = \frac{(\Delta T \bullet F)^2}{L} \tag{4.5}$$

$$R = \frac{2L}{\Delta T} - \frac{\Delta T}{2C} \tag{4.6}$$

while F is defined by

$$F = \frac{1}{2}(\sqrt{\delta^2 + 1} - \delta) \tag{4.7}$$

where

v = rated voltage of switch (user specified)

i = rated current of switch (user specificied)

δ = damping factor (typically 0.9)

The equation also assures that energy lost in the capacitor Cv^2 when the switch goes from "OFF" to "ON" is equal to the energy lost in the inductor $Li^2/2$ when the switch goes from "ON" to "OFF" state, thereby minimizing losses.

The above approach is the method used to simulate all components found in the small-time step library of the RTDS.

4.4.2 VSC Bridge Configuration (Small Time Step)

The small time-step circuit constructed in RSCAD for the interface of the PV system with main network is given below in Figure 4.9. The circuit consists of the small-time step VSC T-line branch, the 2-Level VSC bridge, three-phase reactor in series with resistance, high pass filter branch and the VSC interface transformer branch.

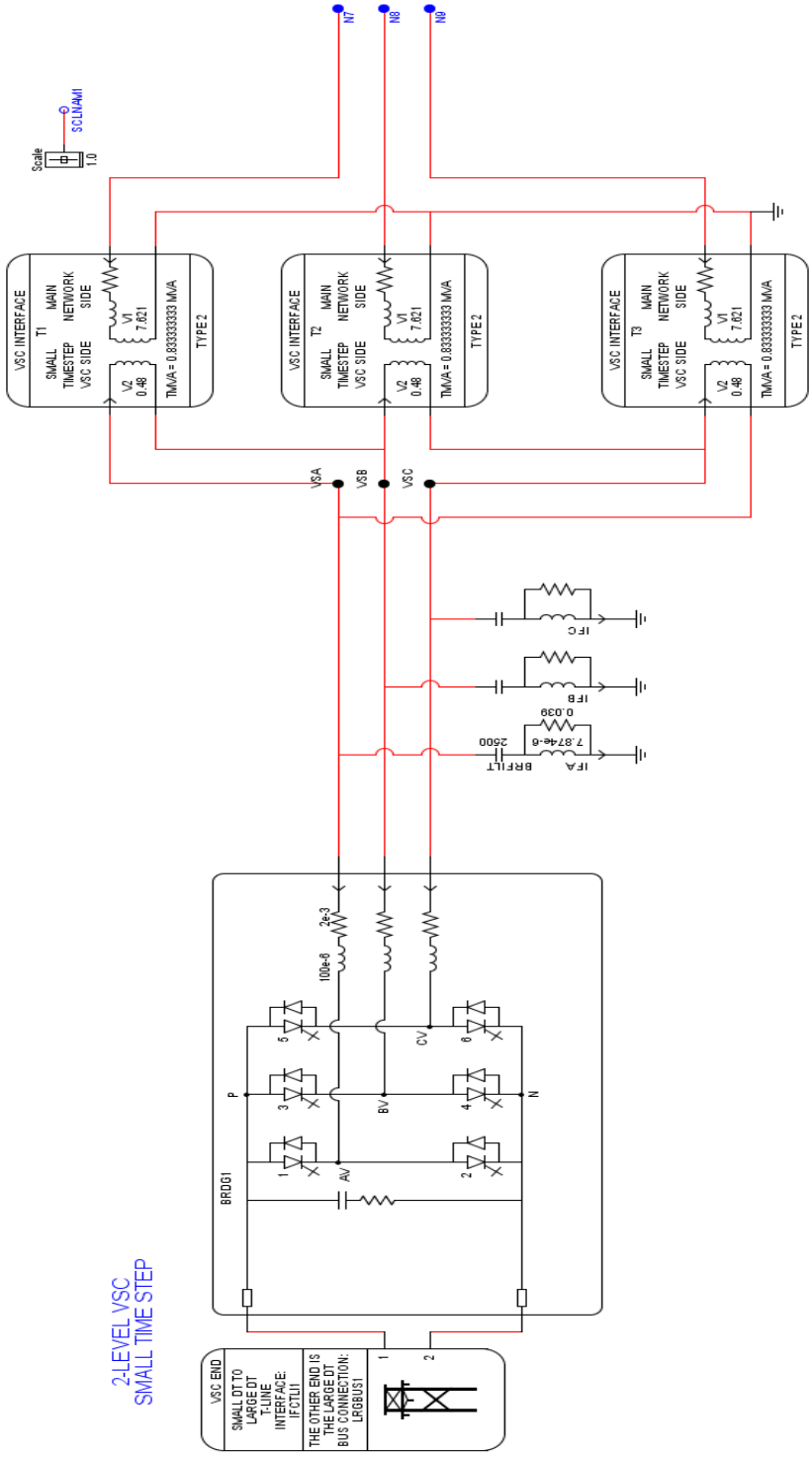

Figure 4.9. Small time circuit for VSC Interface of PV System [25].

The VSC receives large time step (50µs) inputs from the PV array system through the small-time step VSC T-line model.

Six-Pulse Bridge

DC voltage from the PV is converted into AC through the VSC Bridge. The firing pulses for the components in the bridge are provided by the VSC bridge firing blocks and will be discussed shortly. A closer look at the VSC bridge is shown in Figure 4.9.

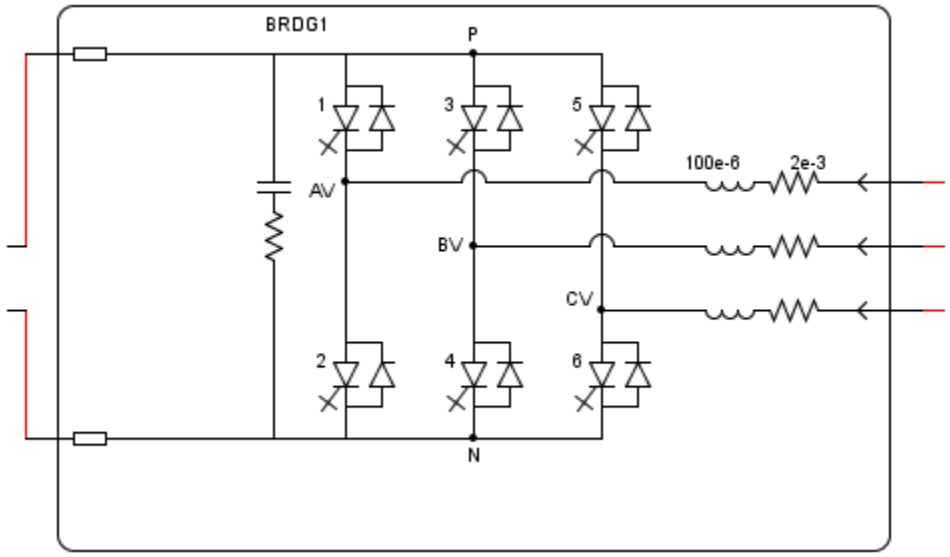

Figure 4.10. VSC BRIDGE.

Filter

The output of the VSC bridge is filtered for higher order harmonics generated by fast switching of the VSC valves through the hipass filter branch. Switching of power electronic switches occur at frequencies over 1200Hz [25]. These will cause excessive generation of current & voltage harmonics around the switching frequencies, and the hipass filter will act as a short circuit at these harmonic frequencies and effectively minimize the impact on the main network side. The hipass filter is shown in Figure 4.11 below.

The grid filter parameters are calculated using the following equations [6]:

$$Xfilt = \frac{V_{bus}(LL_{rms}) * V_{bus}(LL_{rms})}{MVA(\ filter\ )} \tag{4.8}$$

$$Cfilt = \frac{1}{Xfilt\,(2 * pi * fgrid\,)} \tag{4.9}$$

$$Lfilt = \frac{1}{Cfilt\,(2 * pi * fresonance) * (2 * pi * fresonance)} \tag{4.10}$$

$$Rfilt = (2 * pi * fresonance) * Lfilt \tag{4.11}$$

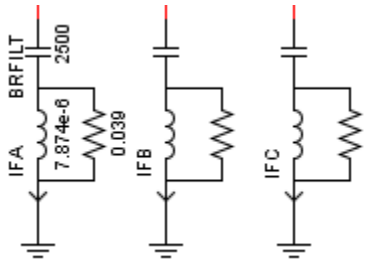

Figure 4.11. HIPASS Filter.

VSC Interface Transformer

Three single-phase transformers are stacked together and connected in a wye-delta configuration to represent the interface between the small-time step subsystem of the simulation and main network (large time step). The transformer parameter details can be found in Appendix A. Figure 4.12 is a representation of one phases of the transformer.

VSC Bridge Firing Blocks & Measurements

High resolution firing pulses are produced in VSC small time step through the use of VSC firing pulse generation blocks [25].

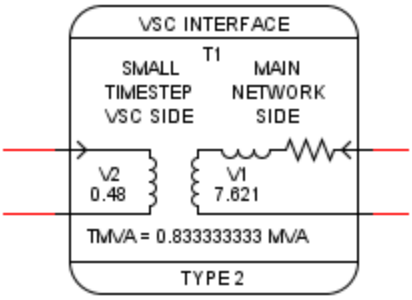

Figure 4.12. VSC Interface Transformer.

Triangle Wave Generator

The high-resolution waves are updated every small-time step and produced by the triangle wave generator. The inputs to the triangle wave generator are

- Triangle wave angle
- Triangle wave omega.

Figure 4.13 is a graphical representation of the triangle wave generator as modeled in the RTDS. Figure 4.14 is a representation of the control block that calculates the triangle wave generator inputs.

Firing Pulse Generator

The high-resolution waves generated by the triangle wave generator are passed on the firing pulse generator. The firing pulse generator has a comparator element which compare the triangle wave output (carrier) with a modulation signal input and generates PWM firing pulse that controls the three-phase VSC bridge. Figure 4.15 shows graphical representation of the firing pulse generator in RSCAD.

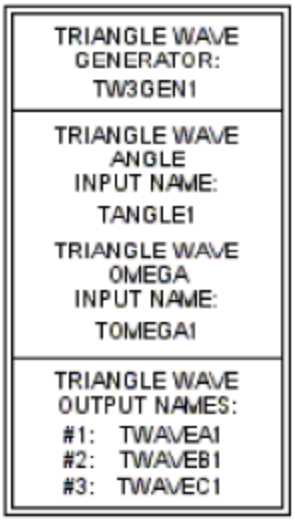

Figure 4.13. Triangle wave Generator.

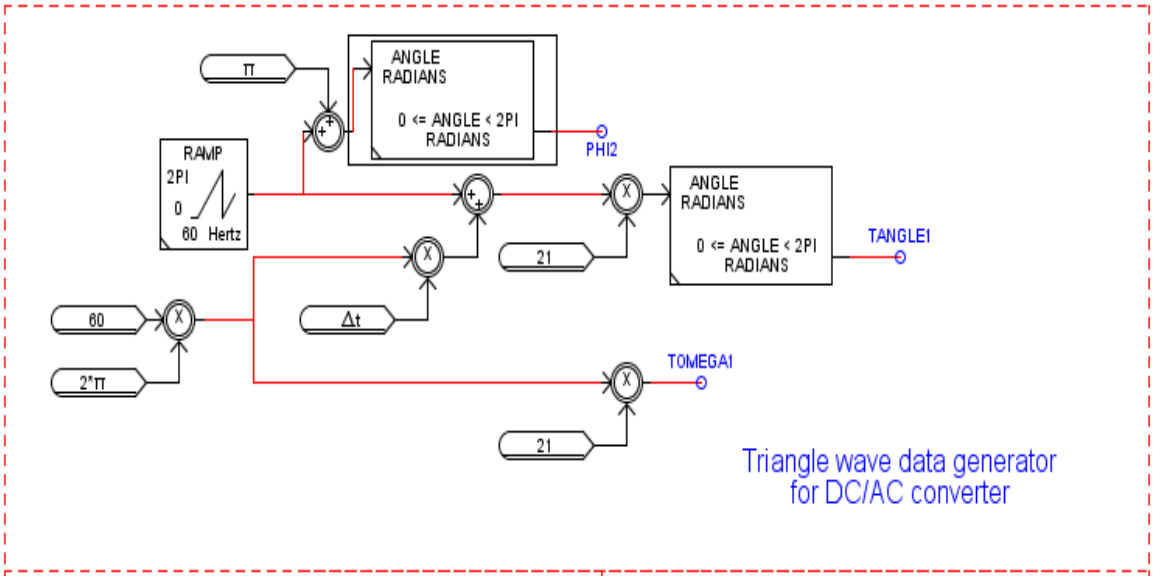

Figure 4.14. Triangle Wave Input Signal Control Block [25].

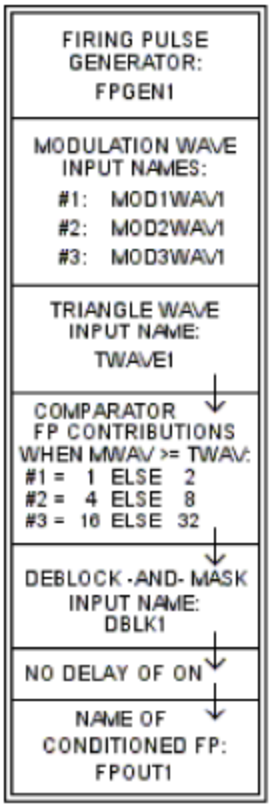

Figure 4.15. Firing Pulse Generator.

4.5 PV System Control

4.5.1 Introduction

The main objective of the PV generation system is to maximize power transfer to the grid at lower quality and reliability conditions that meet the IEEE 929-2000 standard, the PV control system should also have the ability to be de-energized and carry out certain protection protocols during grid faults or under certain grid transient conditions. The PV control system must regulate the power injection to the grid to specified thresholds of power quality and reliability. In this section, the control system of PV system as modeled

in RTDS is discussed, Chapter 5 focuses on the protection of PV generation system and serves as an introduction to HIL simulation techniques.

4.5.2 Decoupled Current Control

The decoupled current control method is the fundamental method of controlling real and reactive power exchanged between the PV system and the grid [29]. The control of PV system real and reactive power is done in the *dq* reference frame where a reference current signal I_{dref} is compared to measured I_d as seen and I_{qref} is compared to measured I_q as illustrated in Figure 4.16. A phase-locked loop is used to determine the ρ, which represents the phase angle of the grid voltages measured. The phase angle ρ is used for the *abc* to *dq* transformation of the VSC output currents and voltages. The outputs of the decoupled current control serve as modulation signals for the firing pulse generator block discussed in Section 4.3. Figure 4.18 illustrates the PLL & and *abc* to *dq* transformation.

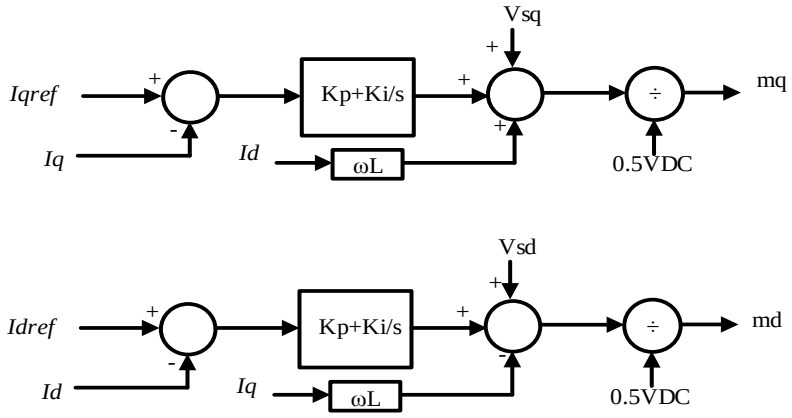

Figure 4.16. Decoupled dq current control [26].

where $\omega = 2\pi \cdot f$, f is the grid frequency of 60 Hz [26].

$$K_p = \frac{L}{\tau_{cc}} \tag{4.12}$$

$$K_i = \frac{R}{\tau_{cc}} \tag{4.13}$$

where τ_{cc} is a design parameter chosen such that the current control bandwidth is smaller than the VSC switching frequency [26]. Other control parameters are discussed in the following sections.

Figures 4.17 are the decoupled current controls as modeled in RSCAD, the parameters for the proportion and integral controls are listed in Appendix B.

Figure 4.19 is a representation of the ABC to *dq* using PLL as implemented in RSCAD DRAFT.

The I_q and I_d of the inverter can be used to independently control the output power of the inverter. The I_d independently controls the real power, while I_q controls the reactive power at the inverter out. The erros between the measure *d*- and *q*-axis currents measured at the inverter output are compared with the *dq* references generated by outer control loops which would be discussed in the next sections. These errors/difference between the reference and the measured values are processed through the PI controller shown and used to produce the modulation signals, m_d and m_q that determine the firing pulses that control the VSC switchings and hence control power outputs. It is important to note that these modulation signals are converted back from the *dq* frame intro *abc*, before they can be used as inputs for the comparator in the firing pulse generator.

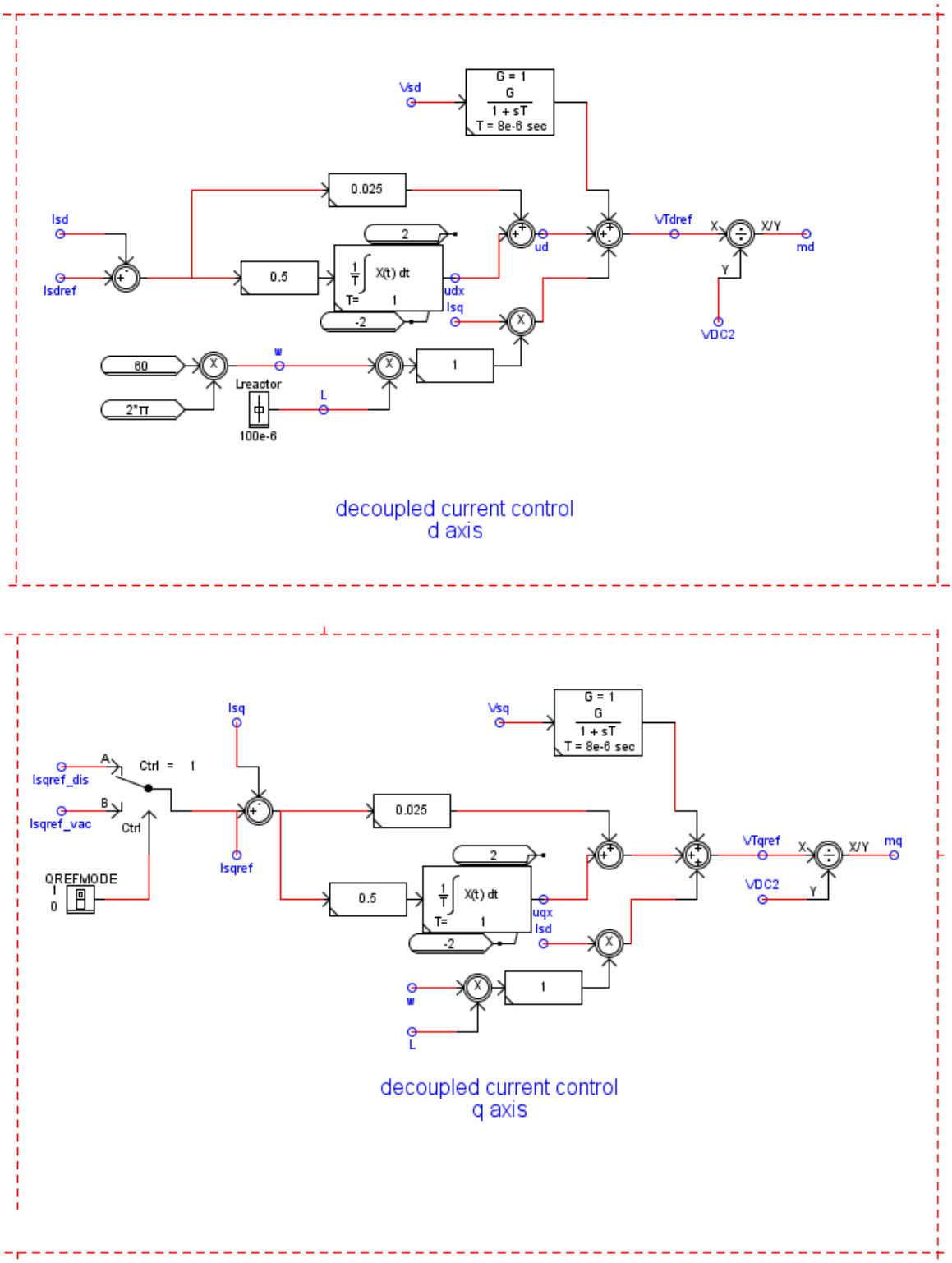

Figures 4.17. Decoupled *dq* current control as implemented in RSCAD [25].

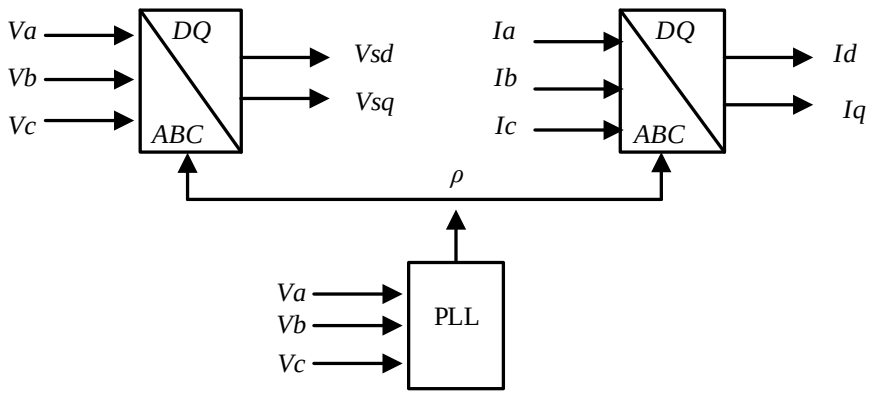

Figure 4.18. *abc* to *dq* using PLL [26].

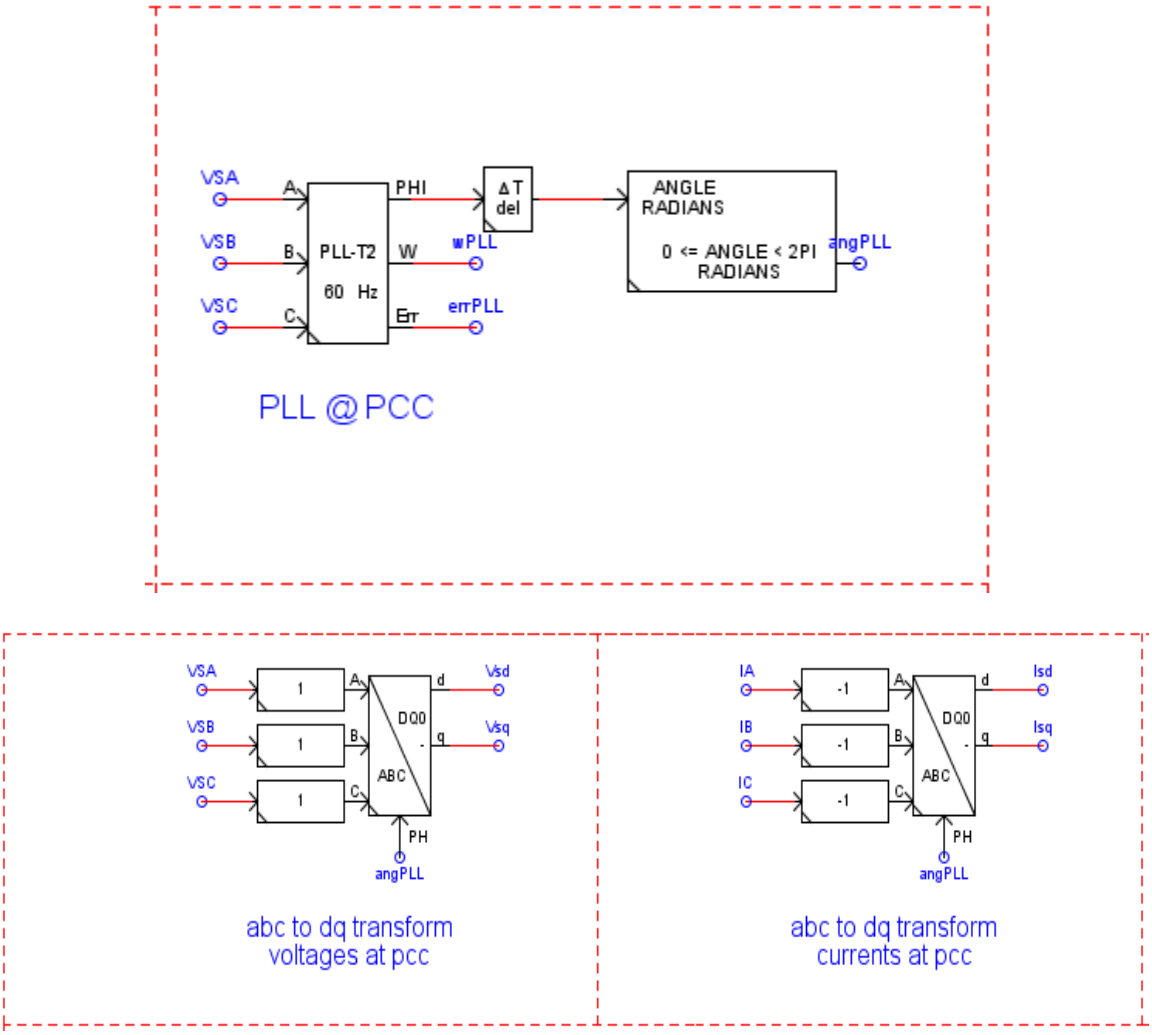

Figure 4.19: Transformation of *abc* to *dq* and PLL implemented in RSCAD DRAFT [25].

4.5.3 MPPT and DC Bus Voltage Control

As stated in Section 4.5.1, one of the main objectives of the PV system control system is control power exchange between the PV system and the grid. The I_{dref} parameter as seen in the decoupled current control is responsible for controlling the real power output of the inverter. In order to maximize output from the PV system, the DC bus voltage must be controlled based on a reference value of the maximum power available from the PV array.

Output of the PV array, other than solar cell properties, depends on the irradiance and temperature [25]. To achieve this a maximum power point tracking (MPPT) method is implemented. MPPT is a method of converting incident solar energy into electrical energy at a very high efficiency [25]. Extensive research has been done in the area of MPPT and several methods have been proposed, the method implemented in the RTDS is the incremental conductance method algorithm. The method is based on the Perturbation & Observation (P&O) method with a slight augmentation to it and widely accepted for implementation of MPPT.

When the array is operating at its maximum power point (MPP), $dP/dV = 0$, which is the soul objective of the MPPT controls. Therefore, if dP/dV is positive, the algorithm seeks to increase the terminal voltage and drive it down to zero, if negative however, the array terminal voltage should be reduced to achieve MPPT [25]. The Hill Climbing method or P&O method achieves MPPT by varying the voltage slightly in this manner at every sample time; however, during rapid changes in environmental conditions, this control method can fail. This had lead up to the Incremental Conductance Algorithm (ICA) Method, the method implemented in the RTDS. The ICA method makes provision for when

the sampled voltage doesn't change from one sample to another. When the voltage doesn't change from one sample to the other, the power output can be varied by an increase or decrease in current and lead to further efficiency of the PV array output.

The flow chart in Figure 4.20 summarizes the incremental conductance algorithm method.

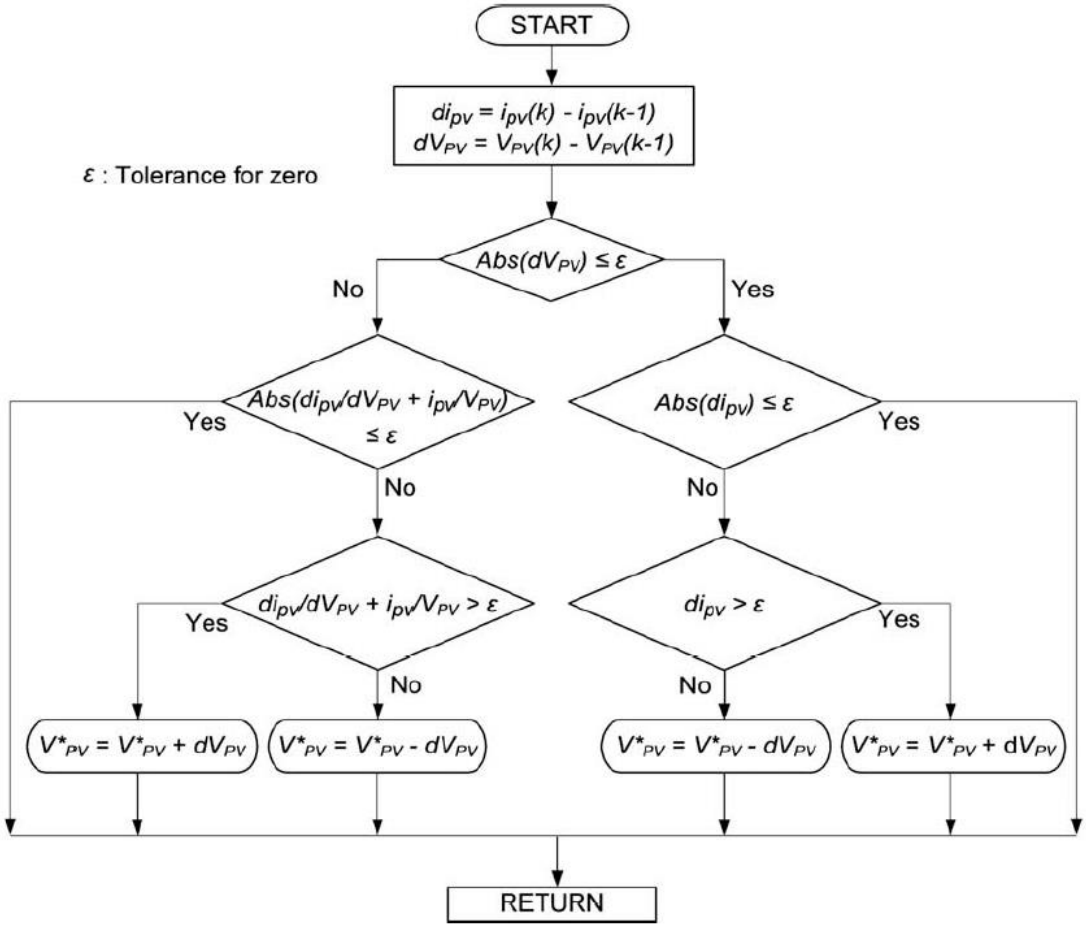

Figure 4.20.: Flow Chart of Incremental Conductance Algorithm method [17].

The MPPT control as Implemented in RSCAD is provided in Figure 4.21. The MPPT control output reference as well as the measure of the DC voltage form an outer PI control loop which regulates the DC bus voltage generates the reference current for the

decoupled current controller. A conceptual representation of this can be seen in Figure 4.22.

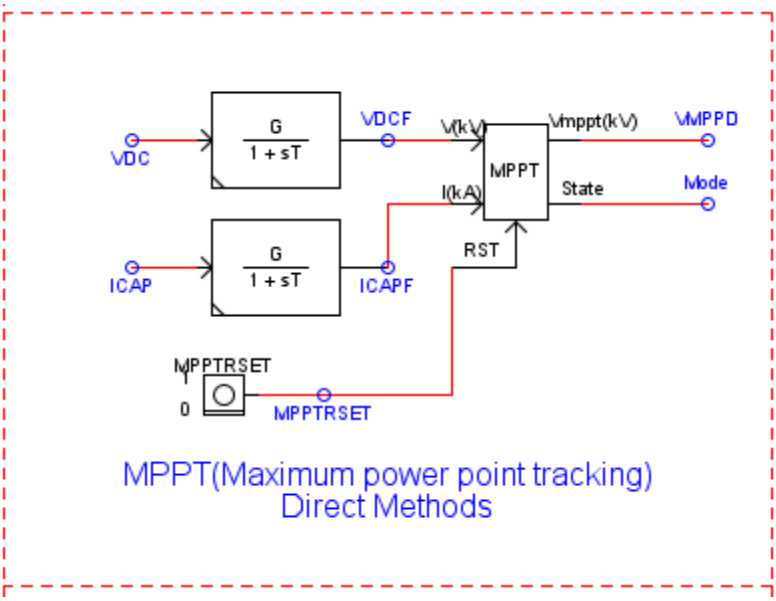

Figure 4.21: MPPT control model implemented in RTDS [25].

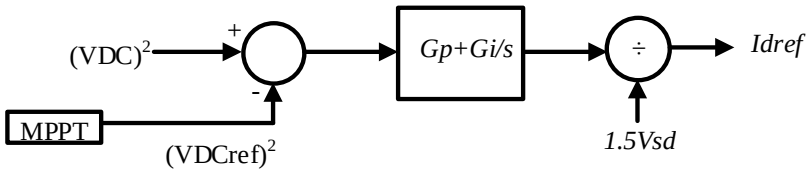

Figure 4.22. DC bus voltage control for I_{dref} [26].

The MPPT generates the desired VDC reference that the PV system should operate on, and this value is compared with the measured VDC and the error is processed through a PI controller to generate a real power output reference. This power reference is divided by the *d*-axis voltage to generate the current reference. The proportional and integral gains (*Gp* and *Gi*) are selected experimentally so that the closed-loop bandwidth of the DC bus voltage control is slower than that of the decoupled current controls [29].

The Figure 4.23 is a schematic of the DC bus voltage control described above as implemented in the RSCAD.

4.5.4 AC Bus Voltage Regulation

Typically the PV system is not allowed to regulate the voltage at the point of common coupling (PCC), as they usually operate at unity power factor, that is the PV system only produces a minimal amount of reactive power. However, in the situation where we have a weak grid, the PV system controls can be designed in a manner which allows it to control the voltage at the PCC (i.e., produce reactive power) up to the PV array reactive power rating. This is one of the applications of a grid-connected PV system. Hence, two different methods can be used to generate the *q*-axis current reference which determines reactive power generated at the inverter output. We could employ a low level controller that simply sets the I_q reference to zero, which implies zero *q*-dispatch and unity power factor, in this case the control structure is trivial. The reference can also be obtained from an AC voltage regulation PI control loop, which would regulate the bus voltage at the PCC between the PV system and the grid by supplying reactive power up to the power limits of the PV array. Figure 4.24 is a block diagram of the AC bus voltage regulator control loop while Figure 4.25 is a representation of setting reactive power dispatch control, and 4.26 are representations of AC bus voltage controls in RSCAD. In AC bus voltage control, we compare the measured V_{sd} to a reference value calculated to be the nominal rating of the grid bus voltage. This allows for determination of how much reactive power capability is available, and the difference is again processed in a PI control loop that determines the new reference I_q that produces reactive power at the inverter output.

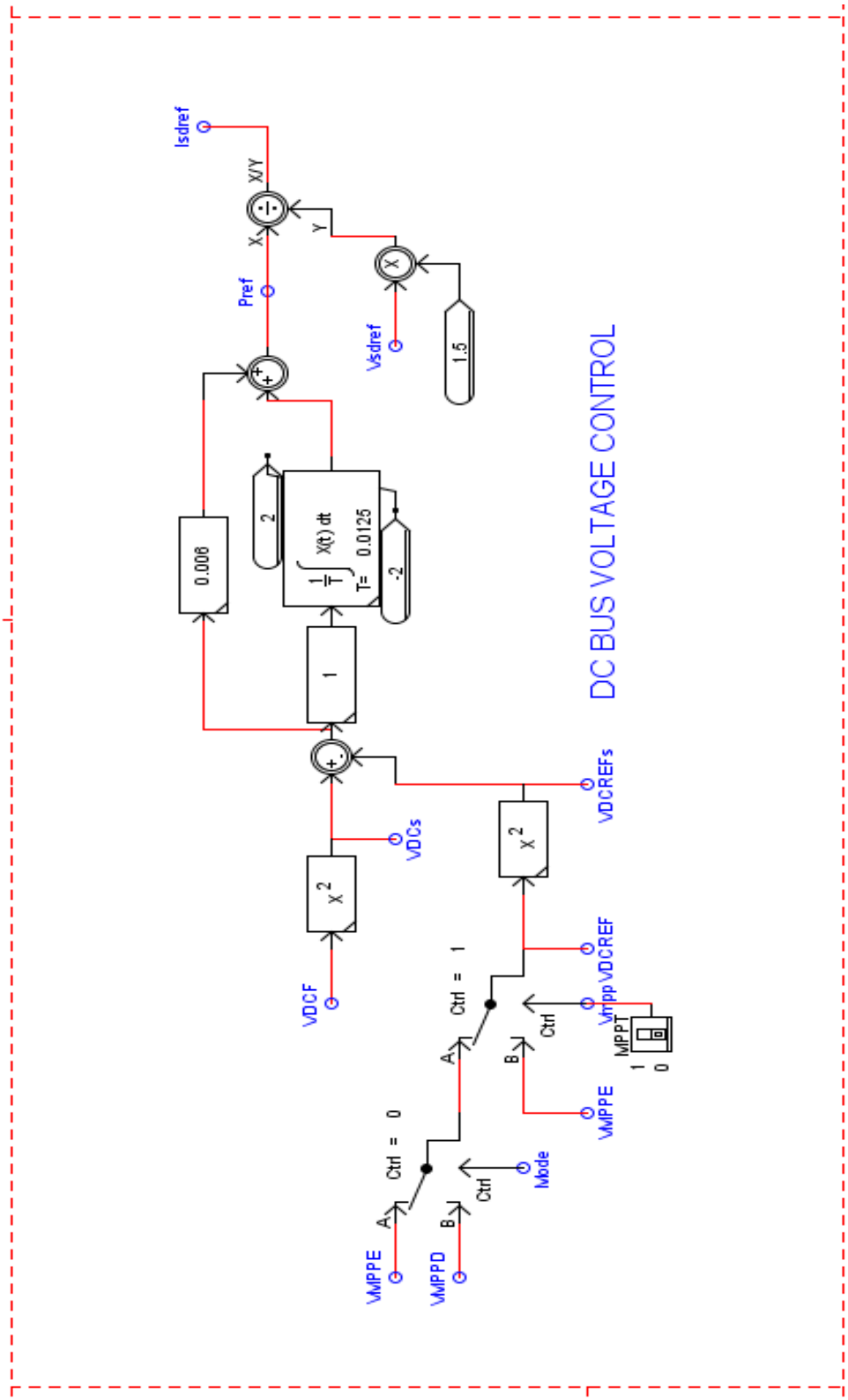

Figure 4.23. Model of DC bus voltage control in RSCAD [25].

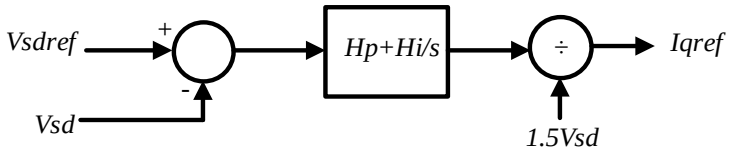

Figure 4.24: Block Diagram of AC bus voltage control for *q*-axis current reference [26].

where

$$Vsd_{ref} = \frac{\sqrt{2}}{\sqrt{3}} V_{rms} \tag{4.14}$$

The proportional and integral gains of the AC bus voltage controls H_p and H_i are one again a function of the closed loop response τ_{cc} of the decoupled *dq* current control as discussed in [29].

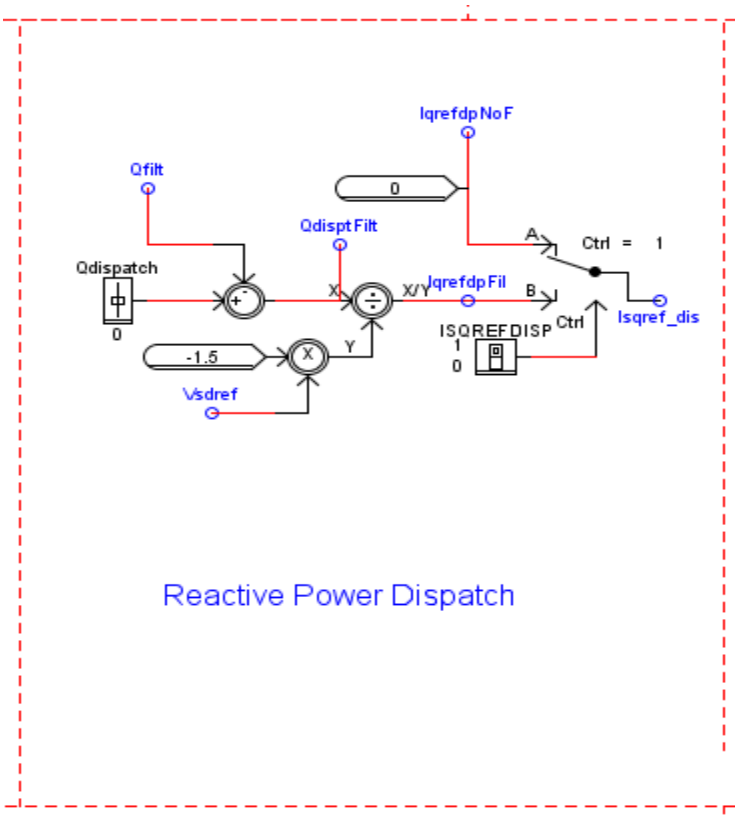

Figure 4.25. Reactive power dispatch (Typically set to zero Q reference) [25].

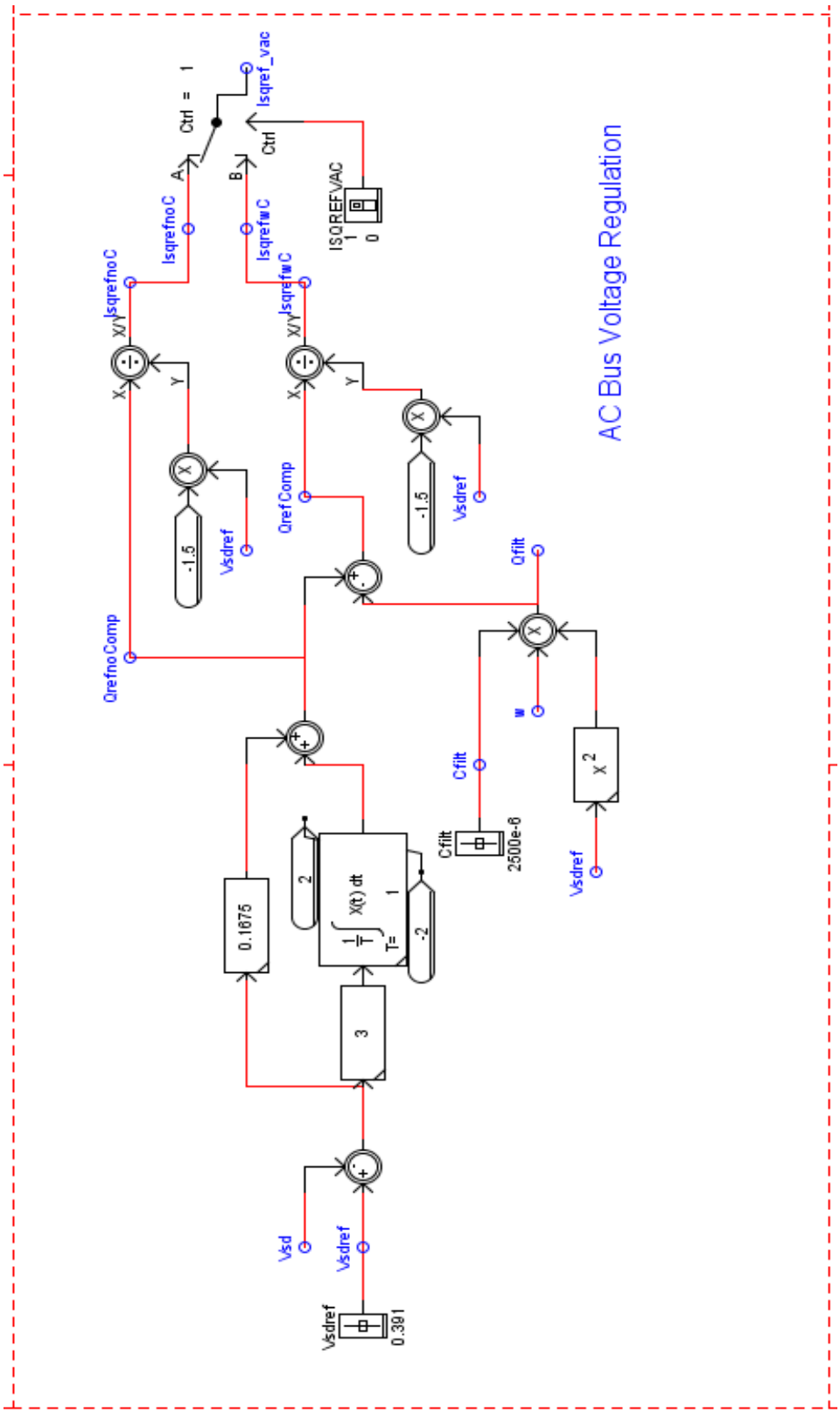

Figure 4.26: AC Bus Voltage Regulation in RSCAD [25].

4.5.5 SPWM

Two different signals m_d and m_q are produced as outputs of the decoupled current control blocks. These signals after being transformed back from *dq* framework to *abc*, serve as inputs to the firing pulse generator firing block, which are compared to the high-resolution output of the triangle wave generator to achieve what is known as Sinusoidal pulse width modulation (SPWM). These SPWM signals are then used as control signals by the firing pulse generator to obtain VSC firing pulses [25].

Consider a representation of one leg of a VSC bridge connected to a load as shown below in Figure 4.27:

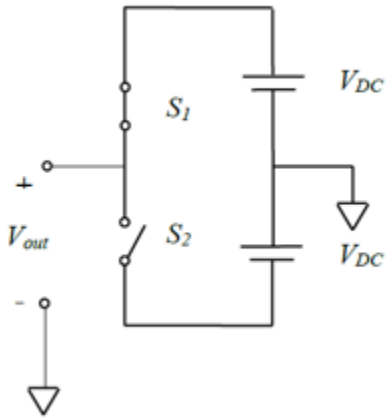

Figure 4.27. One leg of a 2-LEVEL VSC Bridge Topology [25].

The Figure 4.28 represents the the SPWM firing pulse generation sequence described. The sinusoidal signal representing the modulation signal V_m and the triangle wave, representing the output of the triangle wave generator known as the carrier V_c. Therefore the SPWM logic is defined as:

When $V_m > V_c$, S_1 is closed, S_2 is open, V_{out} = +VDC

When $V_m < V_c$, S_1 is open, S_2 is closed, V_{out}= -VDC

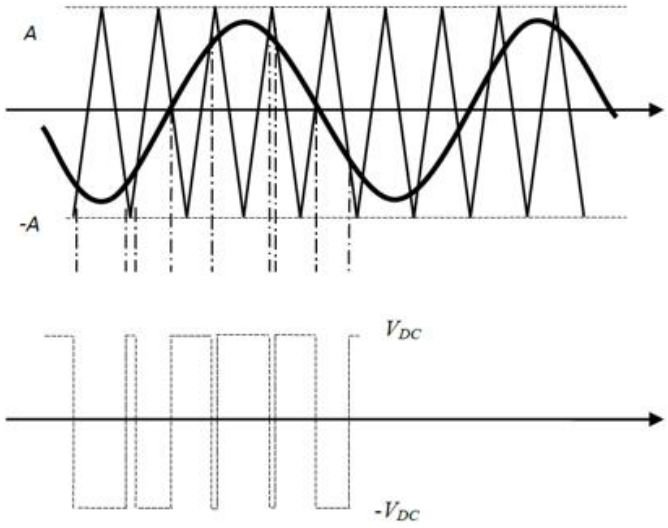

Figure 4.28. Illustration of SPWM [30].

As can be observed from the Figure 4.26 above, When the value of the triangle wave exceeds that of the modulation signal, then the switch above for the corresponding phase leg, will be turned off, conversely when the amplitude of the triangle wave is less than that of the modulation waveform, the switch below for that phase leg will be turned on. For each leg, the switches are prohibited from being turned on at the same time as this will lead to a short across the entire phase. The switching frequency for this VSC bridge model in the RTDS is to 21 * 60 Hz [26].

The control block for generating the firing pulses for the actual VSC bridge implemented in RSCAD is provided in Figure 4.29.

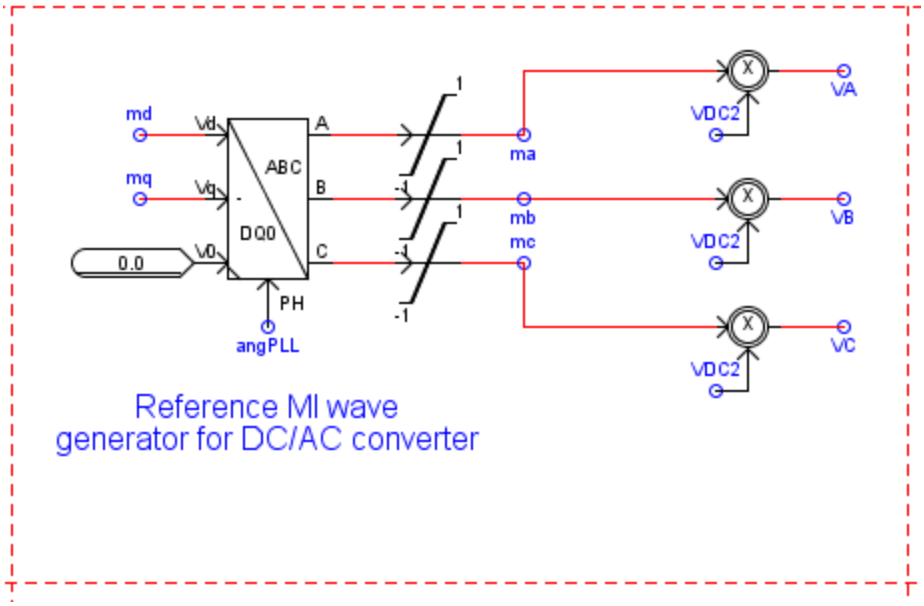

Figure 4.29. Modulation waveform generated in RSCAD [25].

4.6 Analysis of Grid Connected PV System

As discussed in Section 3.1.2, RSCAD software is equipped with graphic-based user interface which allows for the extensive runtime analysis of power systems models built in DRAFT module. The RUNTIME module can be used to visualize results and measurements in real time in form of plots, meters and charts. The RUNTIME module also allows the user to manipulate and vary enabled parameters during runtime and the effects of such changes can also be monitored and captured in real time. This section is composed of analyzing the performance of controls for power exchange between the PV system and the grid as well as the systems response to fault and transient conditions in the grid.

4.6.1 Power Controls Analysis

The soul purpose of our current controls is continually control the real and reactive power injections from the PVC system into the grid. The PV systems are often rated for

operation at unity power factor, which is also a requirement according to IEEE 929-2000 Std that the PV system should operetae at power factor > 0.85 when output is > 10% of the rating. Therefore, our intention is to keep power output of the PV system at unity power factor, which means setting our *q*-axis current reference to zero in our *dq* control famework.

Case I: Base Case

Our base case is an observation of the PV system parameters at reference irradiation and temperature of 1000W/m^2 and 25^{o}C .Figure 4.30 is a plot of power output of the VSC at runtime as seen in the RSCAD RUNTIME, Figure 4.31 is also an instantaneous measurement of perunit P and Q at the VSC output terminals. It can be observed from the plots and measurements that the power factor is kept at close to 0.985, hence near unity power factor.

Case II: Dynamic Variance of Insolation

In the second case, the insolation and temperature of the PV system is varied dynamically over a 20 second period and the power outputs at the VSC is observed to determine the performance of the controls in real time. Figure 4.32 shows the plots of P, Q and insolation of the PV array over a 20-second period. As we can see from the plots, the output power is proportional to variatrion of solar irradiation and response of the PV control systems are effective in maintaining the power factor at the output of the VSC.

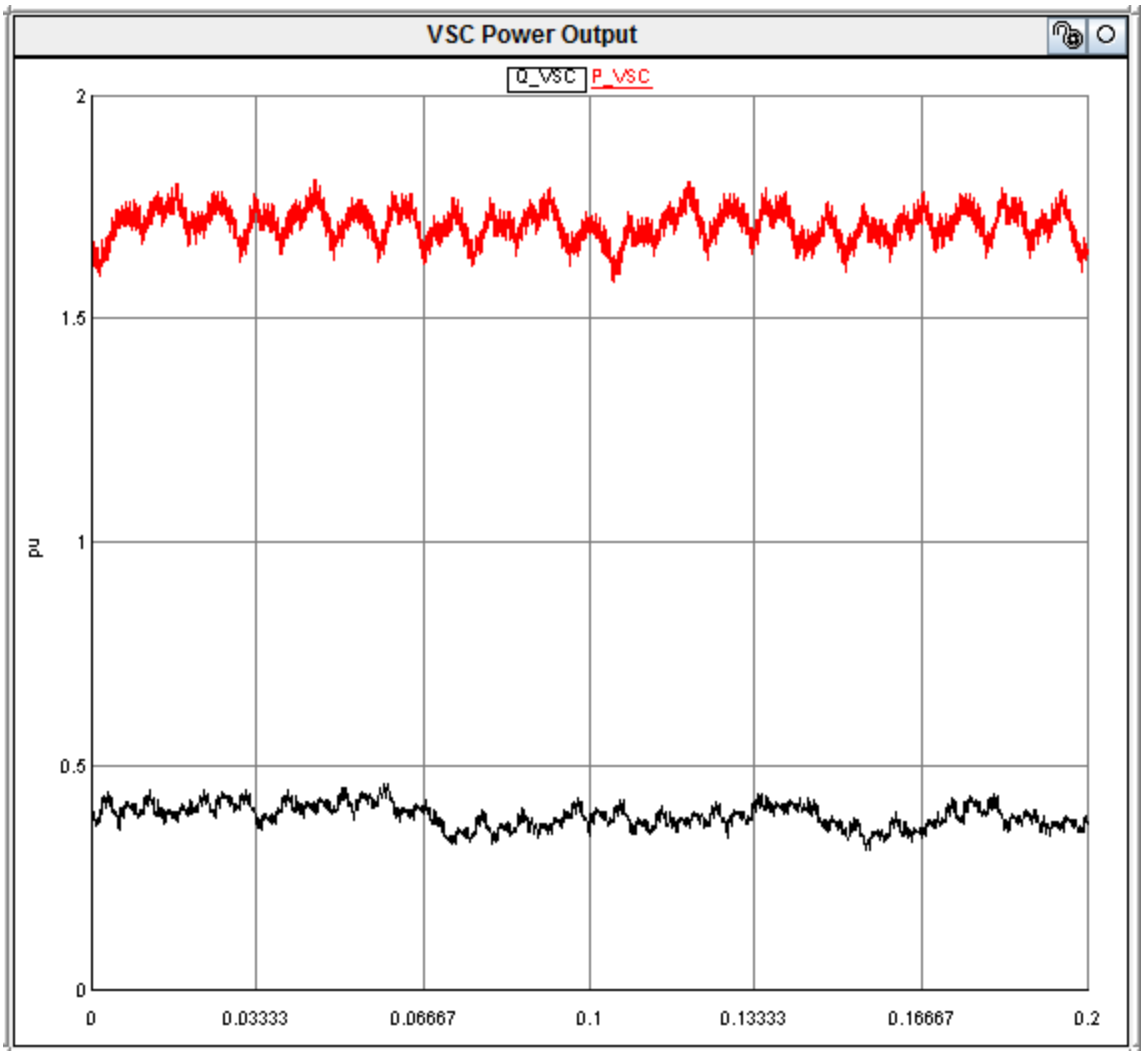

Figure 4.30. VSC Power Output plot, Illustrating power controls.

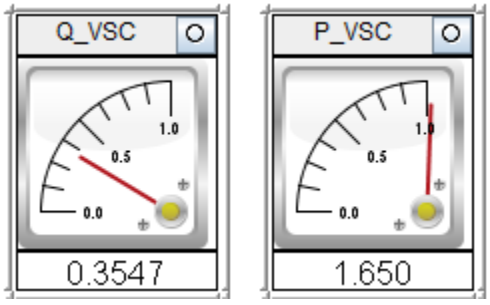

Figure 4.31. Measurements of VSC Power Output in pu.

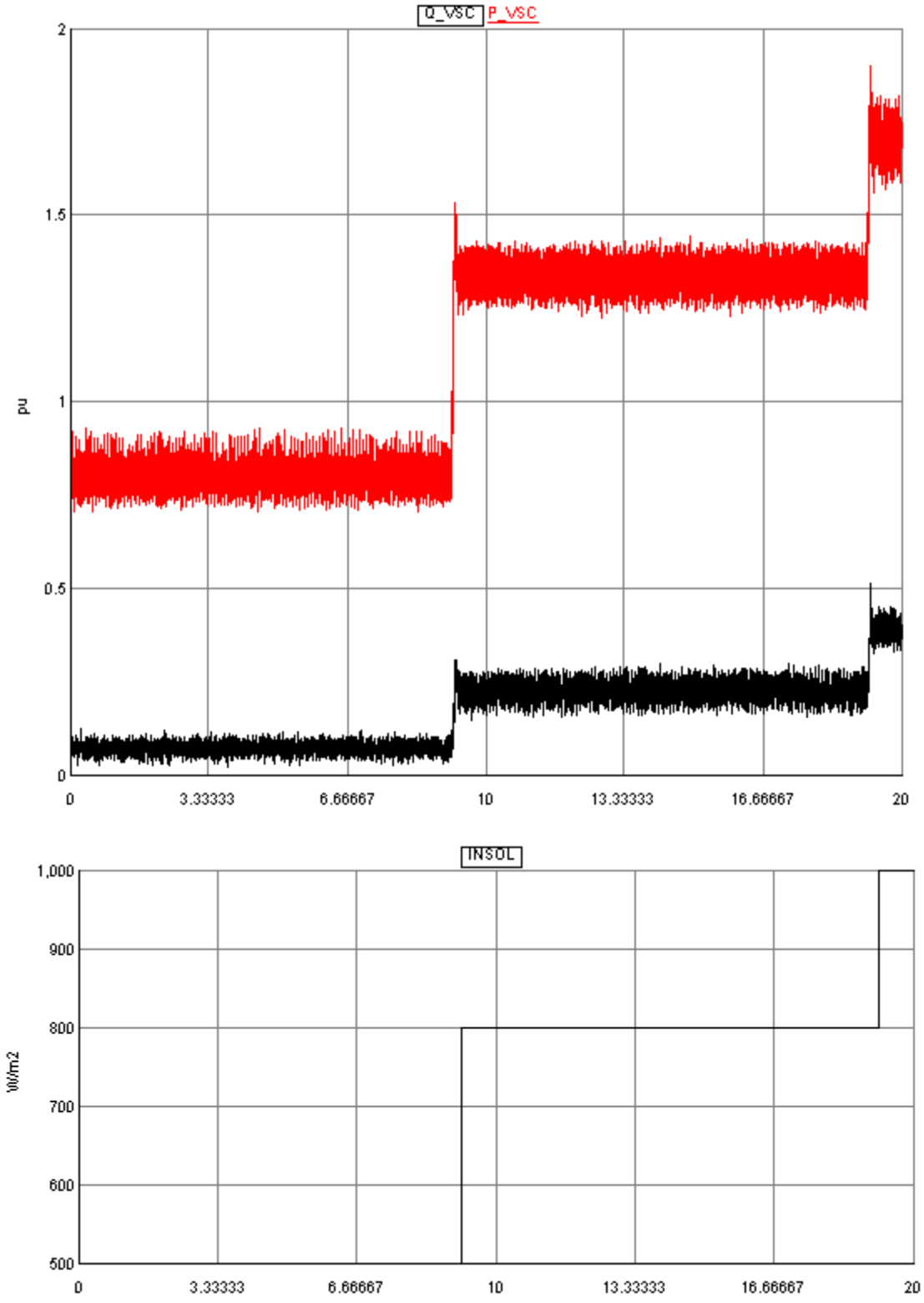

Figure 4.32. Plot of P, Q & Insolation of PV array.

4.6.2 DC Bus Voltage Control

Our control objectives at the DC bus is to keep the voltage as close to the reference as possible. This is accomplished through the MPPT controls discussed earlier in Section 4.5.3. From the plots in Figure 4.33, it can be observed that as insolation is rapidly increased from 200W/m^2 to 1000W/m^2 over a 10s period , the DC voltage reference is adjusted accordingly and the DC bus voltage is controlled to match up almost perfectly with the reference.

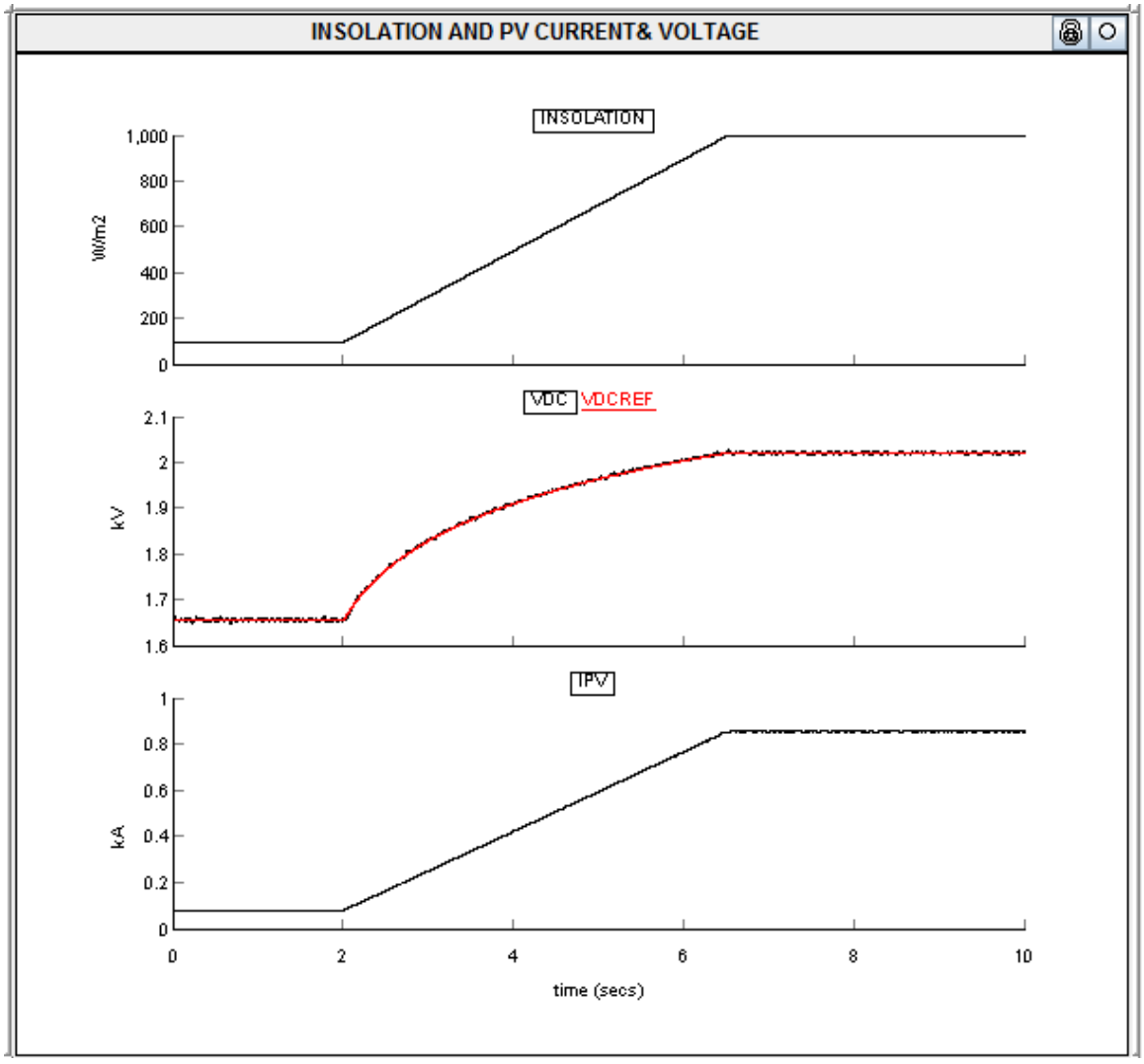

Figure 4.33. Plot of Insolation, PV Voltage and Current Output.

4.6.3 AC Bus Voltage Controls

The objective of the AC bus voltage controls is to essentially keep the voltage at the PCC in phase with the grid, this is achieved through the decoupled *dq* current control that generates firing pulse controls for the VSC. The utility control system frequency and the PV system must operate in synchronism with utility grid at all time. The operating range of the PV system according to IEEE 929-2000 Std should be between 59.3 – 60.5Hz, with a maximum angle difference of 1.2Hz.

In the RTDS, we have invoked the use of an angle difference meter, to measure the phase shift between the grid side and PV system side, and determine the performance of our controls.

Figure 4.34 shows the angle difference measurement configuration in RSCAD DRAFT, and the angle difference measured in runtime which remains at a value < 0.5, demosnstrating synchronization of the system and frequency stability.

Figure 4.35 also details the voltage plots as measured from the VSC side of the transformer and grid side of the transformer, from the plots, it can be observed that the system is in synchronization and operating at rated pu voltage.

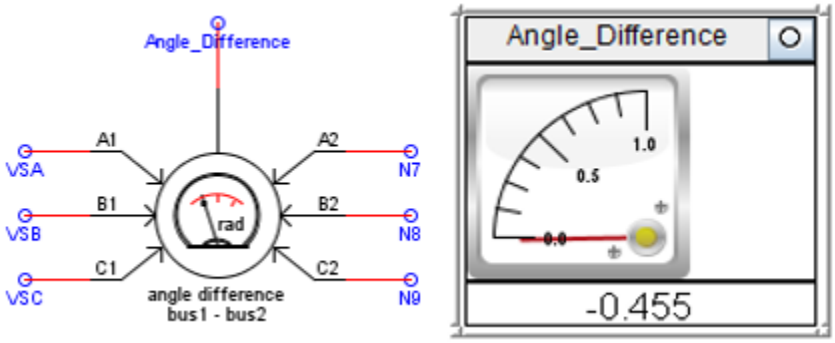

Figure 4.34. Angle difference

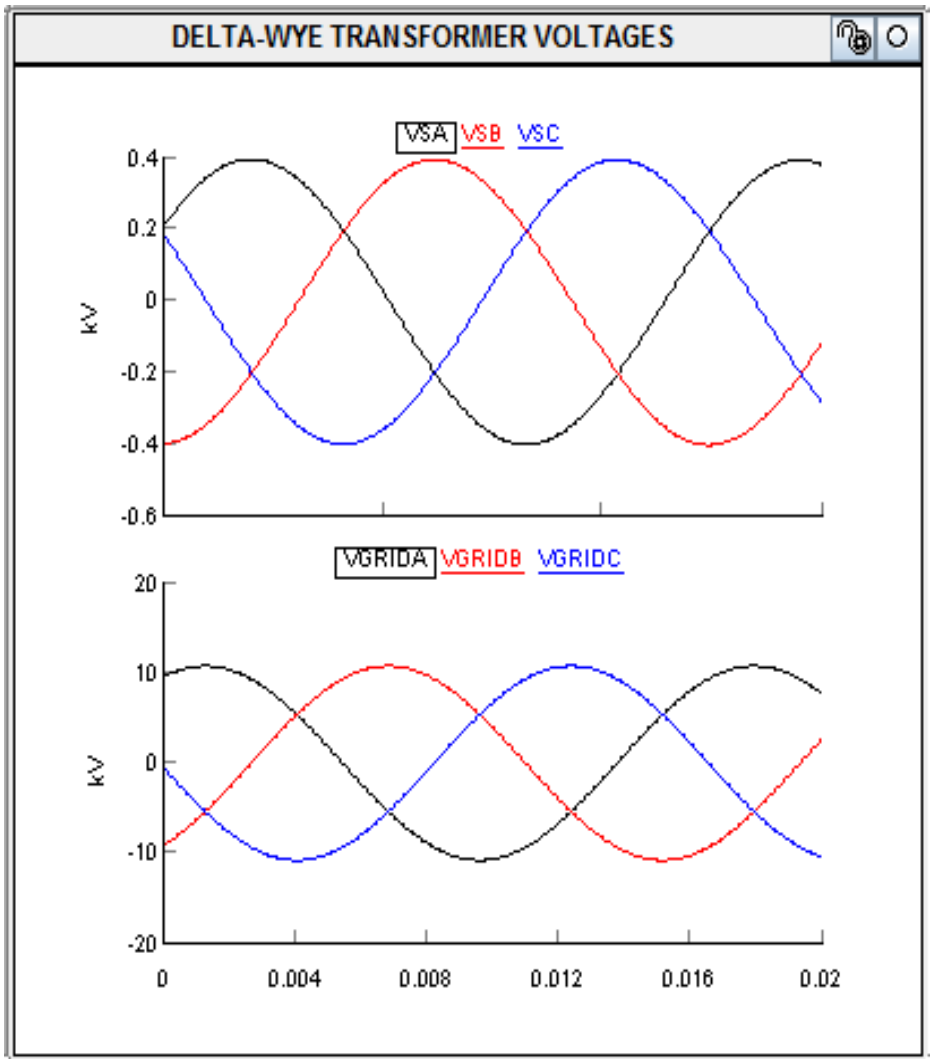

Figure 4.35. Voltage at PCC.

From the plots in Figure 4.35 above, we can observe that at reference PV array insolation and temperature. The voltage at the PCC operates at nominal rated value of on both sides of the transformer. We can also observe from the angle difference monitor that the voltage on both sides of the transformer (Figure 4.34) at the PCC are in synchronization, where N7, N8 and N9 are the grid side bus voltages.

Figure 4.35 shows the pu voltages of the AC side of the system during stable steady conditions. It can also be observed that the voltages are kept at the IEE 929-2000 Std of between 88% ≤ V ≤ 110% during the normal operating conditions.

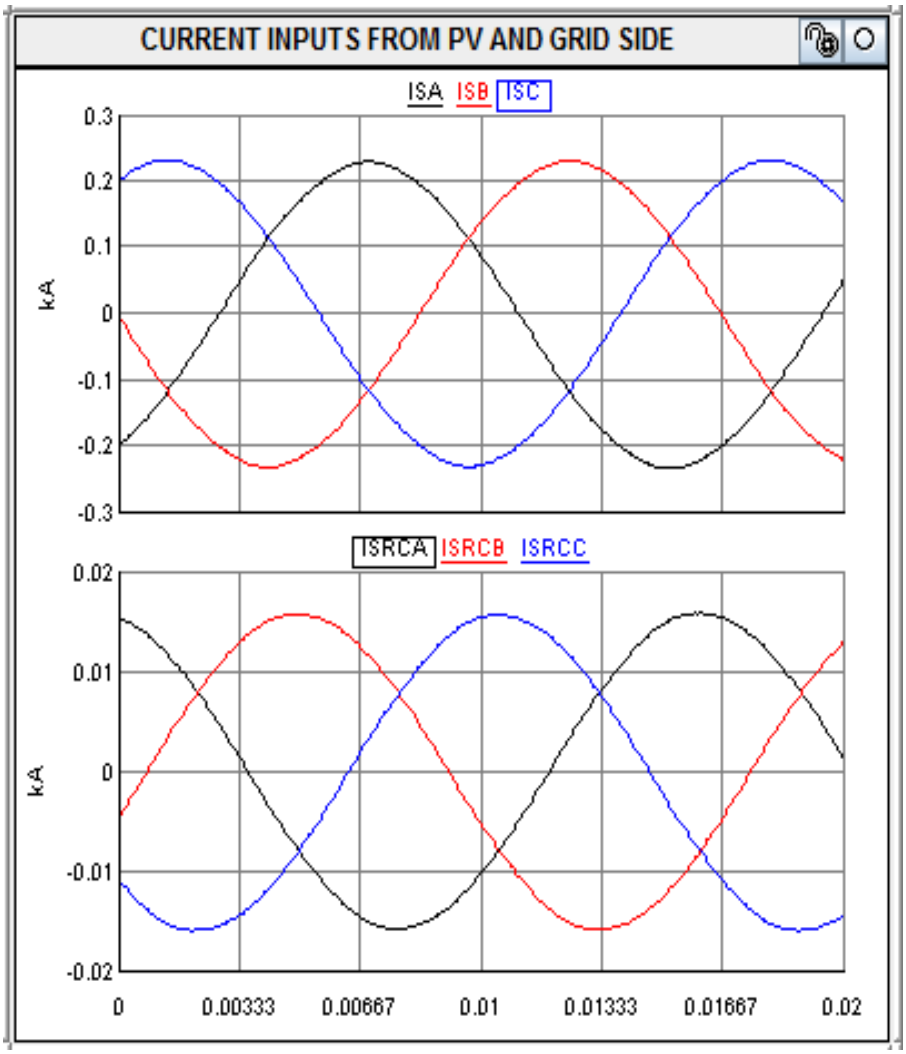

Figure 4.36. Currents at PCC.

In Figure 4.36, it can be observed from the current output of the PV system ISA, ISB, ISC are producing the maximum output current

4.5.4 Transient Analysis of PV System

The grid connected PV system must be equipped with controls that can handle the reliable operation of the PV system during transient conditions such as fault condition or a rapid rise or drop in load conditions. The PV system must detect such conditions and allow for the necessary time delays during short transient disturbances to avoid nuisance tripping [5]. In this section, we simulate a case of short transient conditions (< 60 cycles) and observe the response of the PV system, in order to test the performance of our controls.

Short Circuit Studies (Fault Analysis)

The PV system is equipped to ride through short transient fault conditions that are under 10 cycles, and maintain stability. These conditions are depicted in the fault simulations in Figure 4.37, where a three phase to ground 5 cycle fault is applied to the grid side.

Figure 4.37, is the fault currents measurement, in Figure 4.38 the current measurements at the breaker, and in Figure 4.39 the voltages and in Figure 4.40 the currents through the load breaker during the fault.

The fault controls can be controlled in real time to simulate different types of faults. The dial in Figure 4.37 can be used to selected either a three-phase to a ground fault, or a single line to ground fault. The dial can also be used to choose the specific line (i.e A,B or C) to be faulted. The slider bar bar allows for variation of the fault duration during runtime while the red push button is used to apply the fault manually.

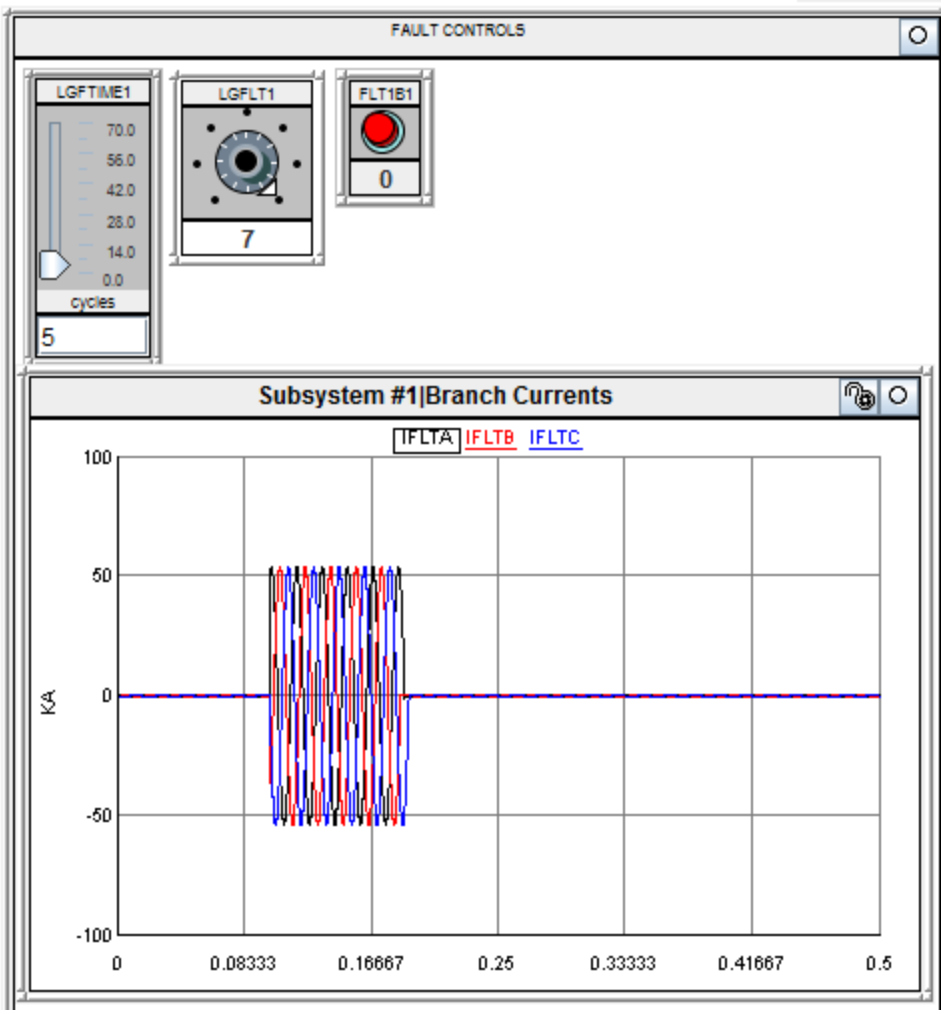

Figure 4.37. Fault Simulation and Fault Currents.

In Figure 4.37, we can observe that a 3-phase to ground fault has been simulated for a duration of 5cycles. The plot shown is a plot of the fault currents measured during runtime. We also able to observe 5cycles of pre-fault before the fault condition is simulated. It is important to note that about 50kA of fault current is measured according to the above plot, however this fault currents are unrealistic and is simply due to the infinite grid source that is modeled. A more realistic source (grid) can be modeled by adding some source impedance to the grid.

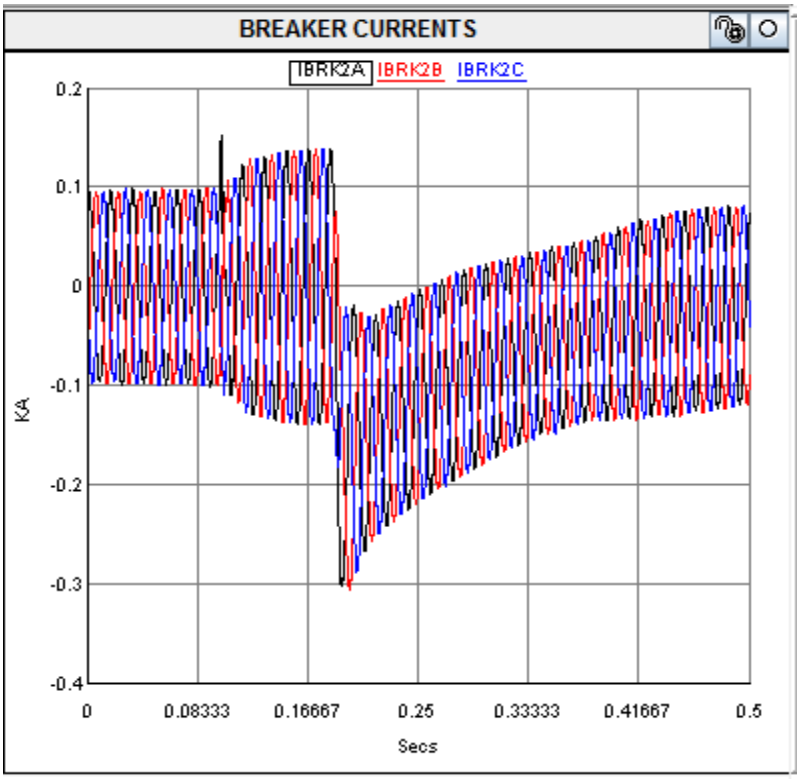

Figure 4.38. Breaker Currents**.**

From the above plots, it can be observed that during the fault duration, the PV system only feeds the fault up to its maximum current, after which it peaks out. At the the end of the fault duration, the PV system controls start to shift back towards normal operating conditttions based on the voltage measurements at the grid. As mentioned earlier, the fault is fed solely through the ideal 13.2kV grid source, with the source impedance kept at 0.1Ω, hence the extremely high peak value of 50kA for fault currents. There is minimal contribution to the fault by the PV because of its non-dispatchable nature. The PV system contributes less than 0.1kA during the fault. After the fault, the PV system controls attempts to restore the system to steady state conditions.

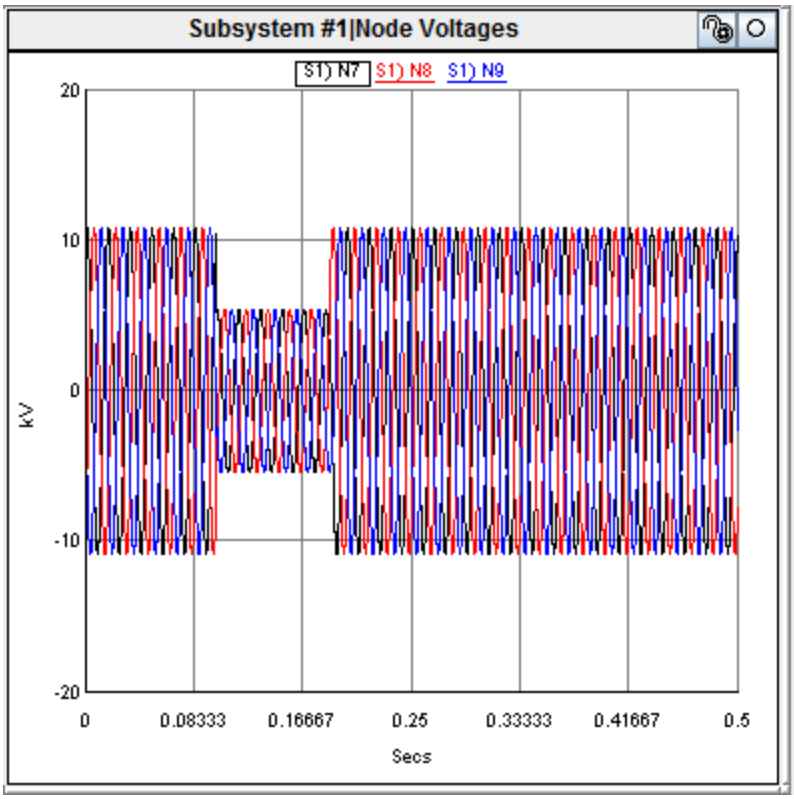

Figure 4.39. Node Voltages at Faulted Bus.

From figure 4.39 above, the node voltages at the faulted bus, it can also be observed that during the fault, the node voltage doesn't collapse completely, this is as a result of the grid strength, and the simulated fault impedance. We can also observe from Figure 4.40 that the current through the load breakers dips quite a bit briefly but there is still current being fed to the load, due to the PV current input and the voltage level at the faulted bus. If a weak grid and zero fault impedance is simulated, it is expected that the voltage at the faulted bus will collapse completely.

In conclusion, from our analysis, it is observed that the PV system controls achieves it's objective of delivering the maximum power available from the array based on the system conditions.

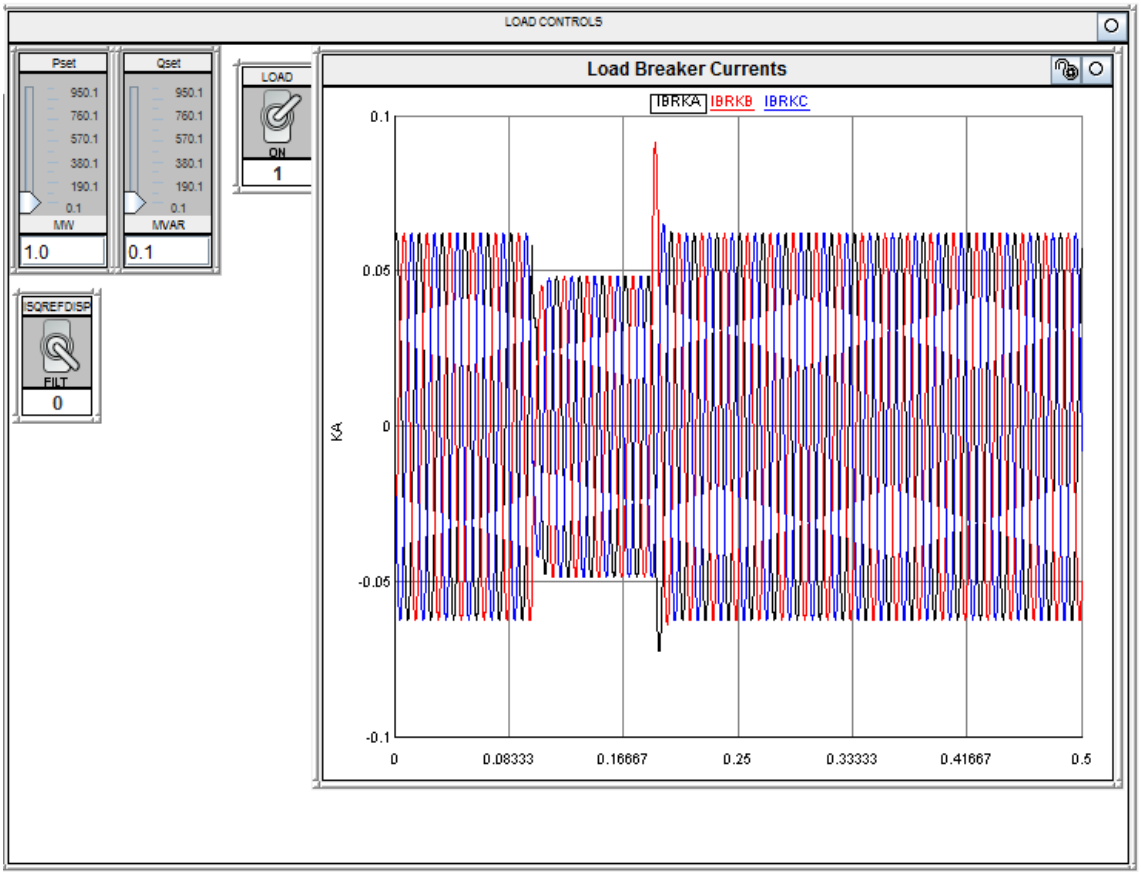

Figure 4.40. Load Current during fault.

CHAPTER FIVE

Hardware-In-Loop Interface of PV System with Protective Relay

5.1 Introduction

One of the major advantages of modeling and simulating power systems in the RTDS is the capability to interface the RTDS to real power system equipment to either test the hardware functionality in real time to validate the operation and reliability of the model. The RTDS as discussed earlier has several methods and protocols by which real equipment or legacy software may be interfaced with the RTDS simulator. This section demonstrates the interface of PV system modeled in the RTDS with a protection device, in order to validate the reliability of our model according to IEEE 1547 standards, as well as test the responsiveness and reliability of the protection device itself.

5.2 Background

Basic protection schemes such as over-current, over- and under-voltage and over- and under-frequency are capable of disconnecting the PV system from the grid during abnormal conditions [17]. However, based on the control system of PV systems, there is only a small amount of fault current contributions from the PV system during a fault. This phenomenon leads to higher non-detection probabilities of PV systems [31]. Therefore, if the PV System supports a local load on the PV side of the transformer, it is imperative that more adaptive protection schemes are designed that are suited to the protection needs of PV system such as anti-islanding protection schemes.

5.3 Description of Simulated HIL Circuit in RTDS

The PV system is being set up for monitoring and protection by a Scweitchzer protection relay commonly used in industry for distribution network protection, the SEL-421 relay. The PV system earlier discussed is slightly modified to include a breaker on the main network side of the VSC interface transformer. Two new components namely CT & PT are also incorporated into the circuit which will be discussed in the following sections. The burden currents and voltages measured at the breaker are sent into the GTAO inputs of the RTDS, the GTAO scales these measurements and the outputs are connected to the low-level test interface of the SEL-421 relay. If a fault or abnormal situation is detected based on the relay settings, the relay detects such events and sends back a digital trip signal to the RTDS through the GTFPI card. Figure 5.1 below is the configuration of the HIL simulation test interface that is discussed in this section.

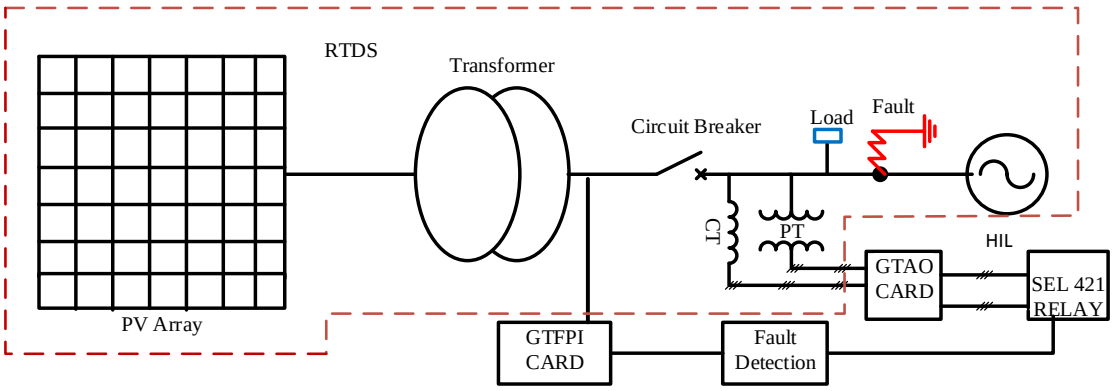

Figure 5.1. Configuration of Hardware-in-loop Simulation.

5.3.1 Instrument Transformers

Instrument transformers are power systems components used for measurement of Grid side voltage & currents and producing relay input level currents and voltages. Figure 5.2 represents RTDS model of current transformer and potential transformer.

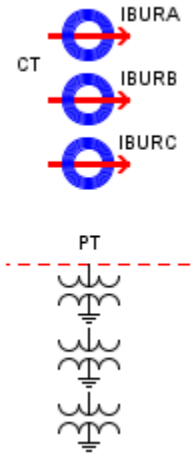

Figure 5.2. Current and Potential Transformer in RTDS.

Monitoring of CT and PT Signals

General for basic protection schemes such as over-current, over- and under-voltage and over- and under-frequency for a PV system, the following signals are monitored during the runtime of the RTDS.

- Breaker currents at point of PCC
- Bus voltage at point of PCC

The currents are then sent as input signals to the CT and PT for measurement. Typically the PT turn's ratio is adjusted so that the secondary voltage is close to 115V RMS.

For our system rated at 13.2kV on the network side, PT turns ratio is calculated as follows

$$PT_{ratio} = \frac{13.2kV}{115V} = 115 \tag{5.1}$$

The CT current output is usually set at 5A RMS and typically the turn's ratio is set at 120 in order to accurately measure the current during fault conditions.

5.3.2 GTAO Interface Card

The GTAO is a high precision analogue output card, with optional 12 pin outputs. The GTAO converts digital signals from the RTDS into analog signals that can be measured through its output pins.

Each channel of the GTAO has a scaling factor which scales the analogue signals to levels desired by the hardware it is interfaced with. The relationship can be expressed by the following equation

$$Analogue(output) = \frac{5V}{G} * RTDS(Signal) \tag{5.2}$$

In order to interface the PV system with the SEL-421 relay, the CT & PT output signals must be sent into the RSCAD representation of the GTAO card as illustrated in Figure 5.3. The outputs of the CT & PT as monitored in the RTDS are IBURA, IBURB and IBURC, and VBURA, VBURB and VBURC, respectively.

Adjusting Scaling Factors of GTAO

The SEL-421 has the capability of low-level test interface as illustrated by Figure 5.4.

In order to interface the relay through the GTAO, the scaling factor of the GTAO output must first be calculated. Therefore, according to Figure 5.4 above, for current:

$$G = \frac{5V}{66.6mV} * 5 = 375 \qquad (5.3)$$

and for voltage:

$$G = \frac{5V}{446mV} * 5 = 375 \qquad (5.4)$$

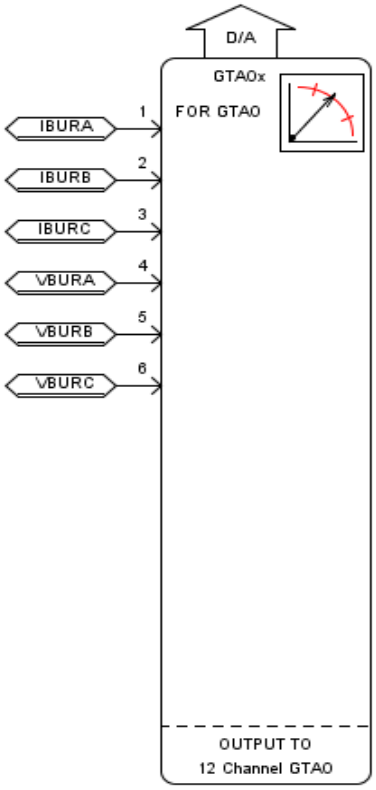

Figure 5.3. GTAO Configuration in RTDS.

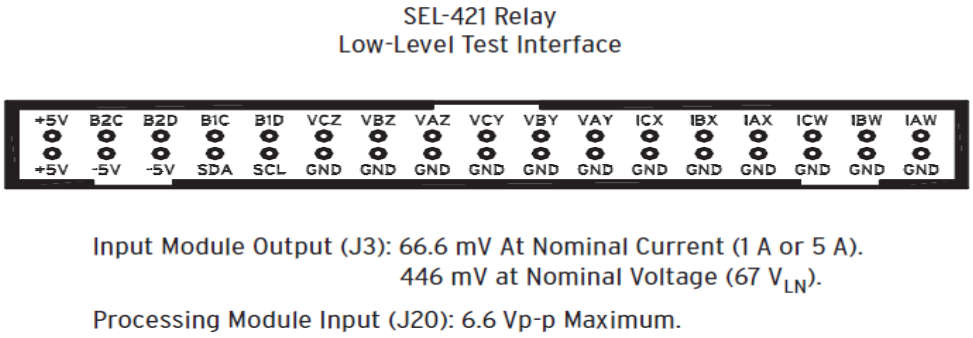

Figure 5.4. SEL-421 Low-Level Test Interface [32].

Figure 5.5 Illustrates the physical connection from the GTAO card mounted on the RTDS, to the low-level test interface of the SEL-421.

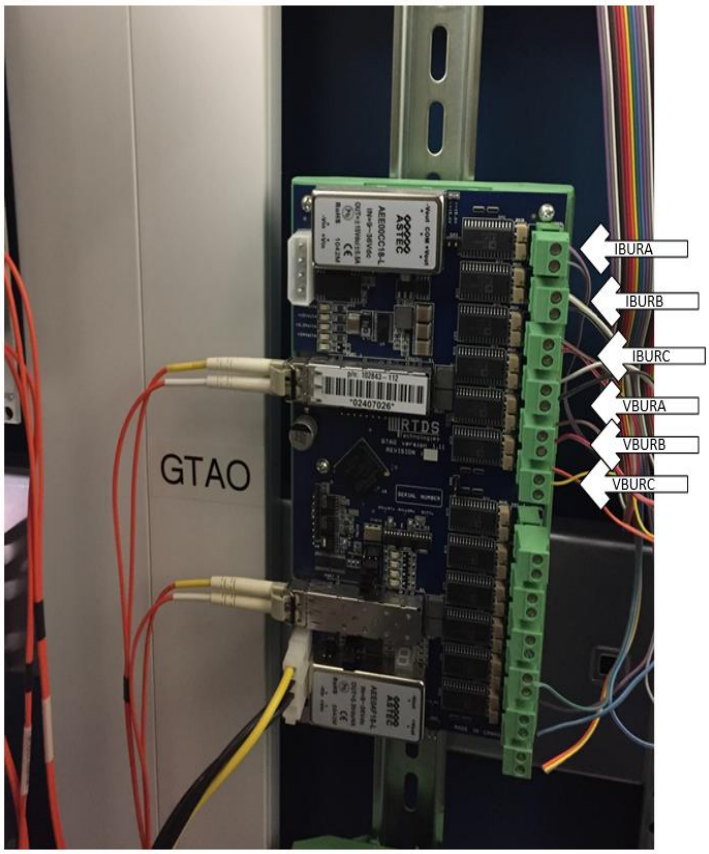

Figure 5.5. Physical Connection of GTAO to SEL-421 Interface.

5.4 SEL AcSELerator QuickSet® Software and Relay Settings

Communication between the SEL AcSELerator Quickset software, and the relay is done via Ethernet cable connection. Details of acquiring the software and setting up the communication protocols can be found in [32].

The IEEE 929-2000 standard, has certain conditions for abnormal voltages and frequencies. It is our primary objective to test the SEL-421 relays ability to maintain these standard conditions as can be seen in Table 5.1 below.

Table 5.1. Response to Adnormal Voltages & Frequency

Voltage at PCC	Maximum trip time
V < 50%	6 Cycles
88% ≤ V≤ 110%	Normal Operation
50% < V< 88%	120 Cycles
137% ≤ V	2 Cycles
110% < V< 137%	120 Cycles
Frequency at PCC	Maximum trip time
F < 59.3	2 Cycles
59.3 ≤ F 60.5	Normal conditions

5.4.1 Relay Settings

The SEL 421 relay would be used to implement virtual over and under voltage protection schemes as well as over and under frequency protection schemes for the PV system modeled in Chapter 4. The Line configurations are based on the rating of the PV

system's CT and PT configurations discussed in the previous section, the line configuration setting for the relay are depicted as shown in the Figure 5.6 below.

The relay configuration is set up for under and over frequency protection using ANSI standard 81 elements as shown in Figure 5.7, with three different levels of pickup to comply with the recommended standards as shown in Table 5.1.

The relay configurations for the under and over voltage protection are implemented with the ANSI standard 27 elements and 59 elements, respectively. The settings for both of these protection schemes are implemented according to the IEEE 929-2000 standard as depicted in Table 5.1. The Figures 5.8 and 5.9 represent the 27 (Under Voltage) and 59 (Over Voltage) elements settings in the SEL-421 quickset software.

A summary of the relay settings used to implement testing of the protection schem can be found in Table 5.2 below.

Table 5.2. Relay Settings

Parameter	*Under Voltage* **(27)**	*Over Voltage(59)*	*Under-Frequency* **(81)**
Trip Signal	271P2T	592P2T	81D1T
No. of Cycles/Sec	10 Cycles	120Cycles	0.5Secs
Treshold Value	7.2kV(Vpeak)	11.7kV(Vpeak)	59.3Hz
Nominal Value	10.7kV(Vpeak)	10.7kV(Vpeak)	60Hz

5.5 HIL Simulation Results

In the following simulation test cases we wish to test the under-voltage (27 Element), over-voltage (59 Element) and under-frequency (81 Element) settings of the relay. We will compare the currents through our breaker and CT to those measured by the relay at the time of the events to demonstrate effectiveness of the protection scheme.

5.5.1 Pre-Fault Conditions

The Figures 5.6 and 5.7 below demonstrate the measurements in the RSCAD runtime and the Human Machine Interface (HMI).

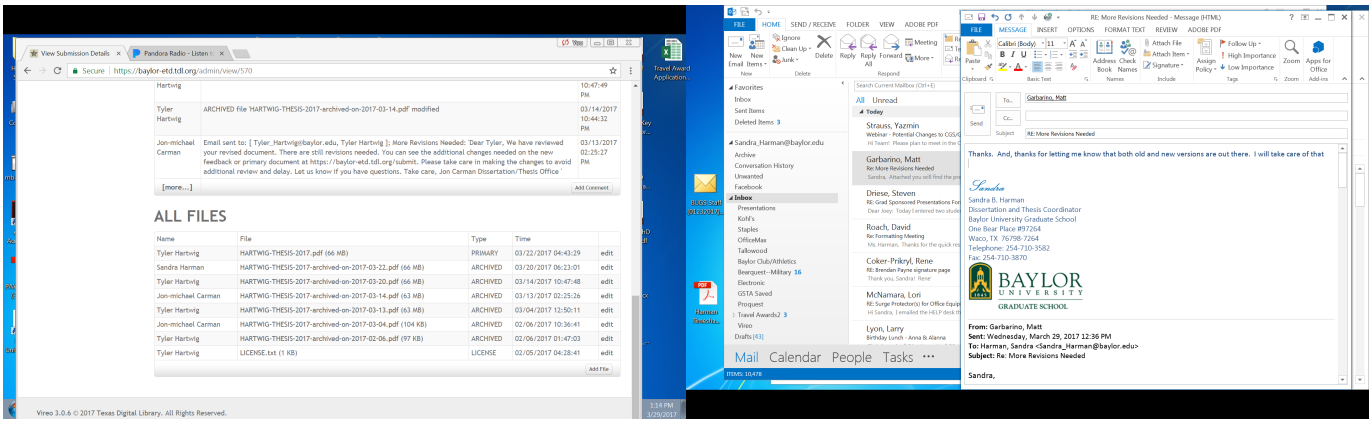

Figure 5.6. Line Voltage and Current at the PCC.

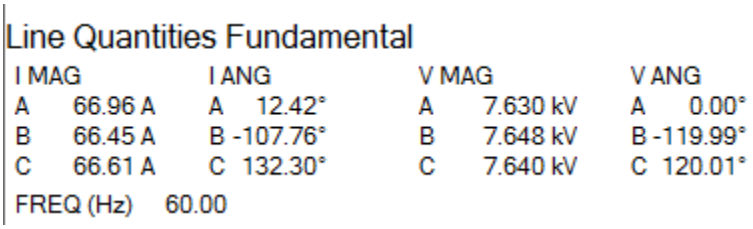

Figure 5.7. Line Measurements as seen in the HMI.

The plots below in Figures 5.8 and 5.9 are pre-fault voltages and currents across the faulted bus and through the breaker. We can also compare these values to those measured in relay and visualized through the HMI, and observe that the GTAO provides accurate D/A measurements.

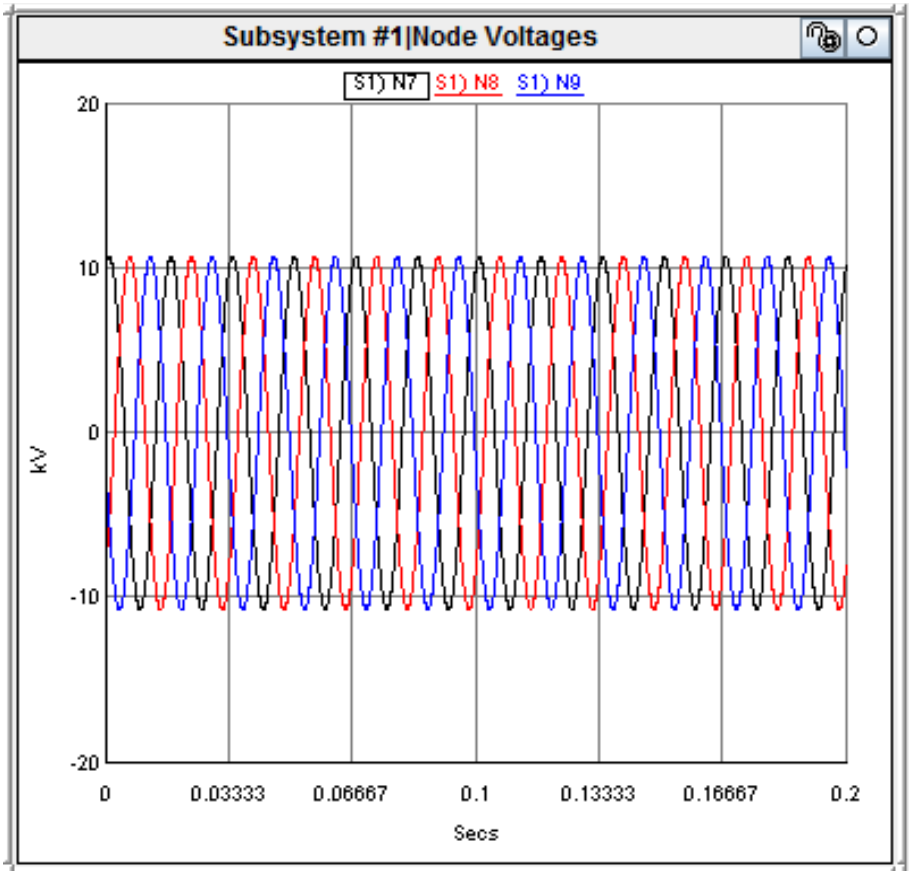

Figure 5.8. Pre-fault Voltage at Faulted Bus.

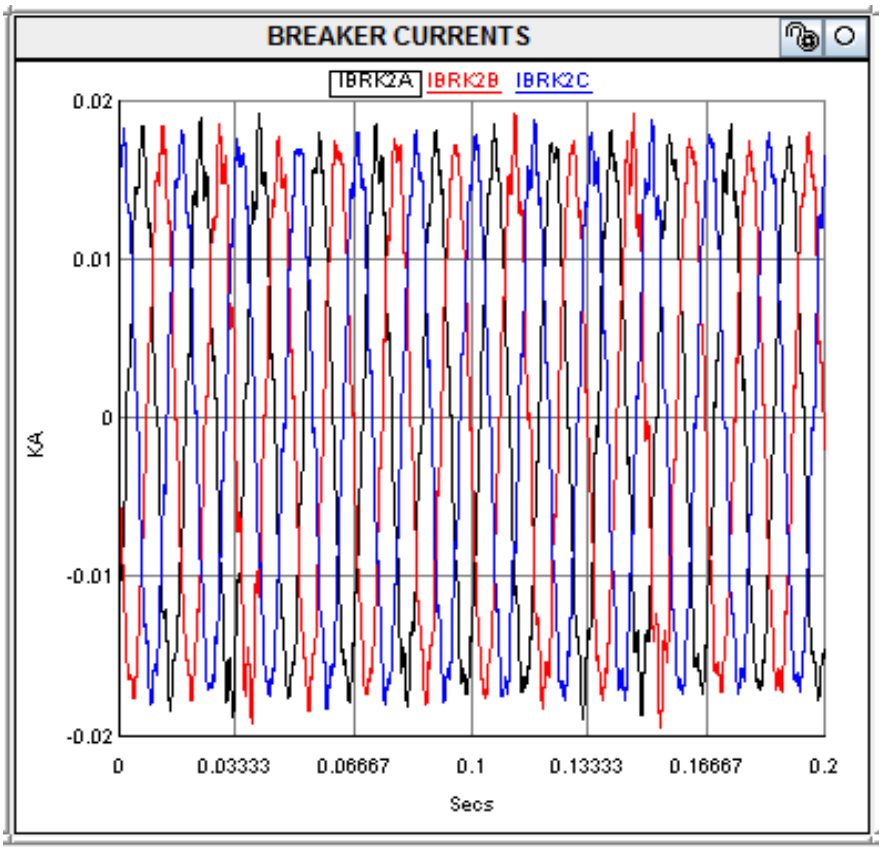

Figure 5.9. Pre-fault Current Measurements at Faulted Bus.

5.5.2 Under-Voltage Protection Simulation

As mentioned in Chapter 5, the designed PV system controls have the ability to ride through short transient conditions; however, if the system equipement is subjected to such maginitudes of fault currents and grid instability, it could be detrimental to the grid. In this section, we show a test for protecting the system against one of the most common form of fault situation, a three-phase to ground fault which results in an under-voltage situation. We wish to observe the voltage measured in the breaker and trip the relay after an undervoltage situation has occurred for more than 10 cycles. The fault simulated earlier in Section 4.5.4 is re-simulated for 65 cycles, and we observe the current through the breakers increase for the duration at which the breaker is closed and then open up after the delay of

10 cycles have elapsed. Figure 5.10 is a plot of the current through the breaker while Figure 5.11 is a plot of the digital trip command that opens up the breaker due to a trip signal received from the relay at the time of the fault.

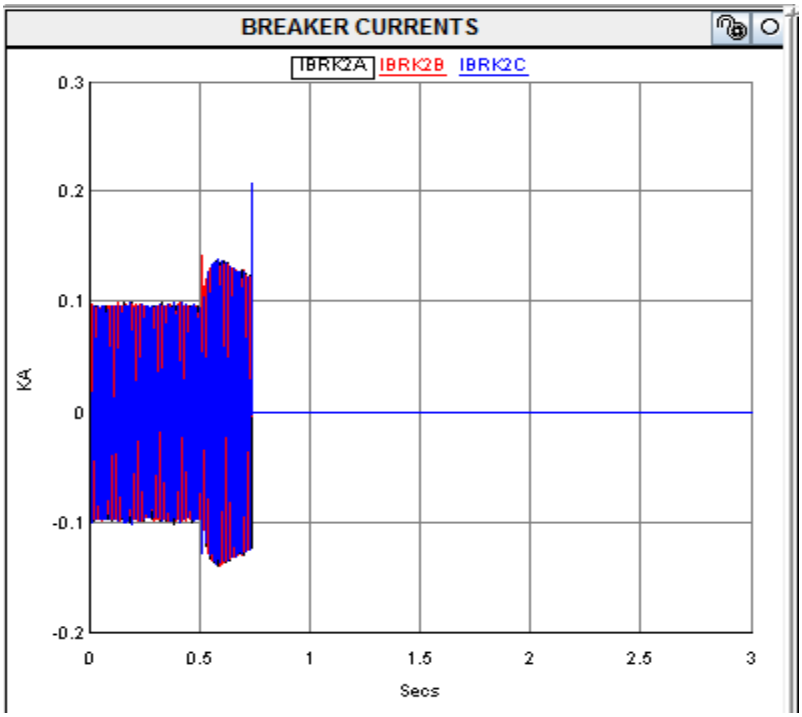

Figure 5.10. Breaker Current measurement.

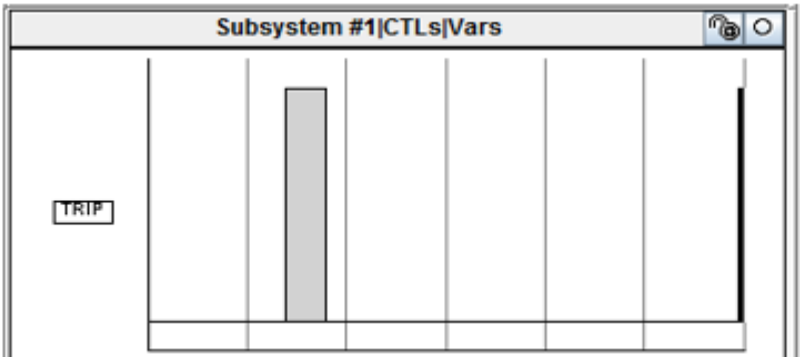

Figure 5.11. Trip Signal.

Figures 5.12 and 5.13 are voltage measurements at the grid bus during the fault and burden voltage at the breaker terminal during the fault. From the bus voltage plot, we can clearly observe an undervoltage situation according to Table 5.1 and Figure 5.8. As soon as the trip signal is applied and the breaker is tripped, the currents through the breaker go to zero, and the voltage measurements through the PT represent the open circuit voltage at breaker.

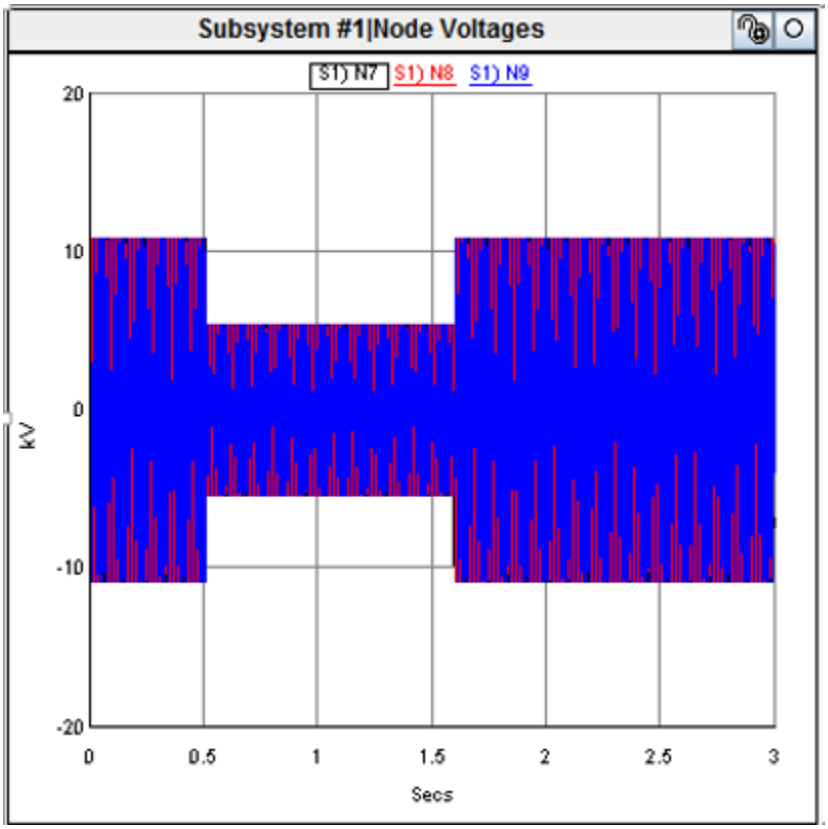

Figure 5.12. Undervoltage at Faulted Bus.

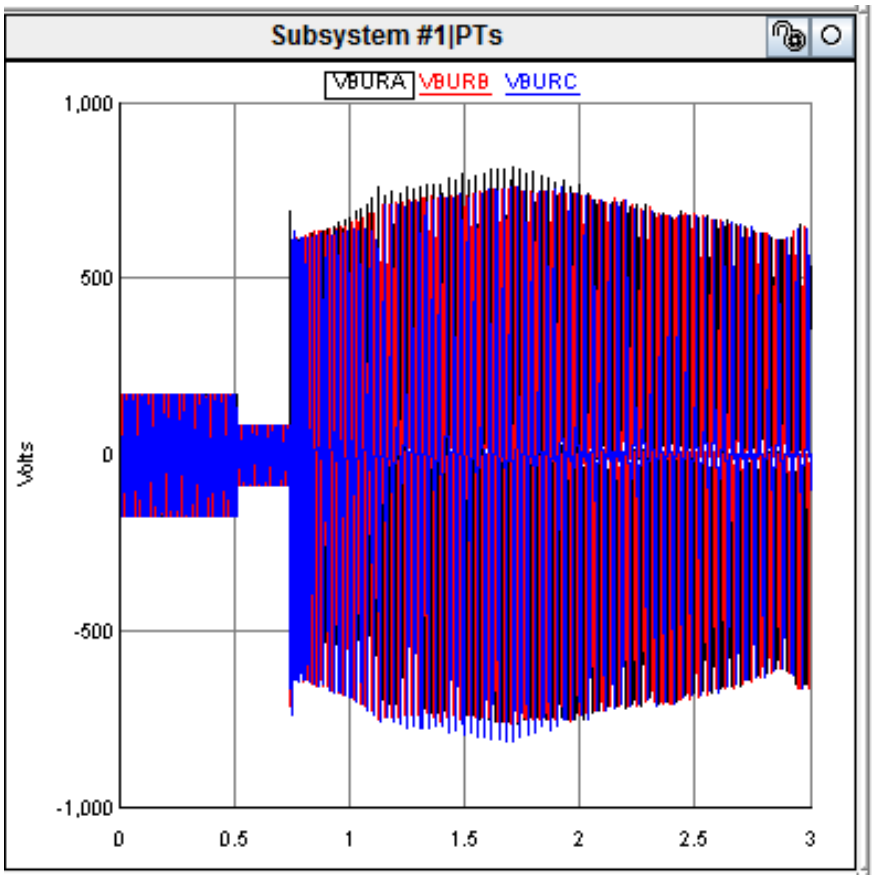

Figure 5.13. Burden Voltage at Breaker Terminal.

Figure 5.14 shows the event log of the trip signal as measured and analyzed in the synchrowave software. Depicting the undervoltage element tripping and showing the accurate details of the trip event as can be observed from the plots in comparison with the plots measure in the RTDS. The voltage drops below the threshold of 50% of the nominal voltage for more than 10 cycles, which causes a trip signal to be sent to the breaker from the relay as seen in the digital plot of the RTDS and the event, where there is a couple of cycles delay between when the breaker is actually tripped in the simulation and when the trip is initiated as shown in plots. This simulation is able to prove our under voltage

protection is capable of executing under the specified period in Table 5.1 for such under voltage conditions.

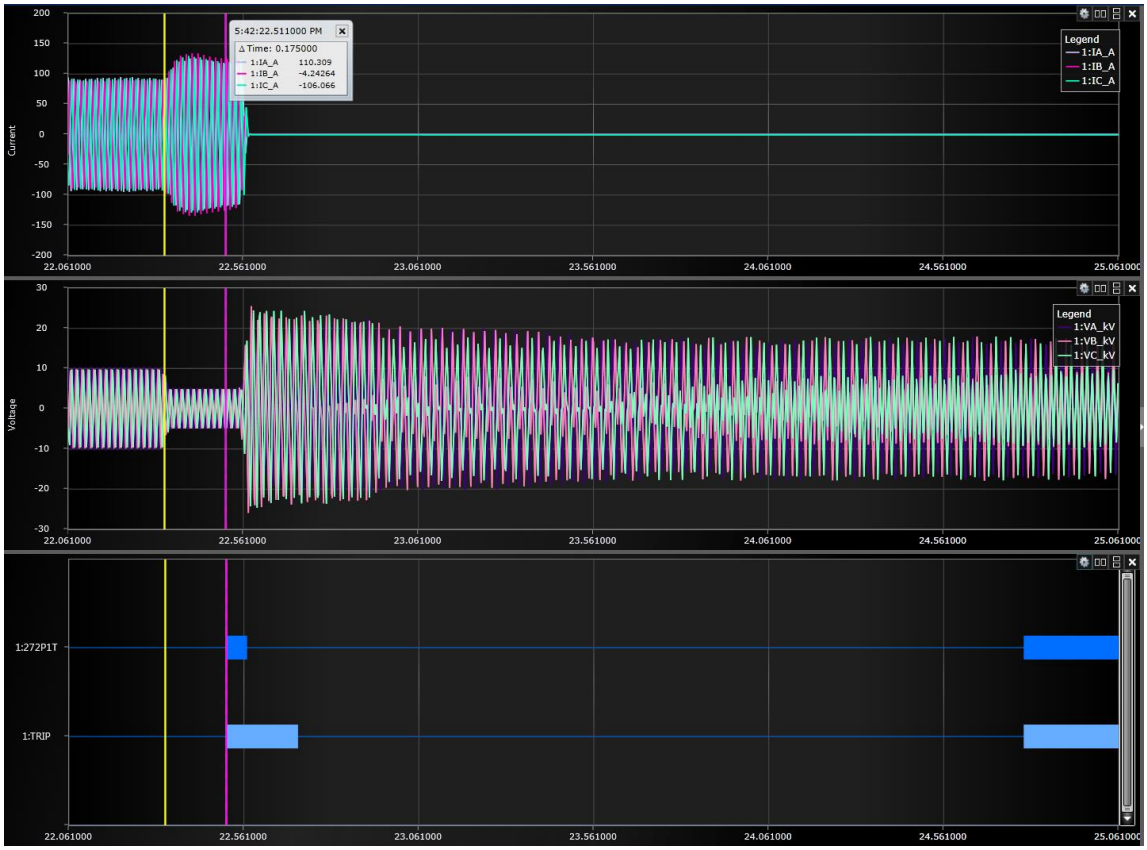

Figure 5.14. Synchrowave Event log of 27 Element Trip.

5.5.3 Over-Voltage Protection

An overvoltage situation is simulated by scaling the source voltage in order to test for over voltages protection, according to conditions in Table 5.2. This results in an over-voltage situation (59 element) being detected in the SEL-421 relay, and a trip signal sent back into the RTDS in order to trip the breaker. Figure 5.15 shows the currents through the breaker during the over-voltage conditions, Figure 5.16 shows the digital trip signal applied to breaker from the realy, Figure 5.17 is a measure of Node voltages at the source that is

scaled, Figure 5.18 is the burden voltages measured, which also initiate the trip signals, and Figure 5.19 is the corresponding event plots.

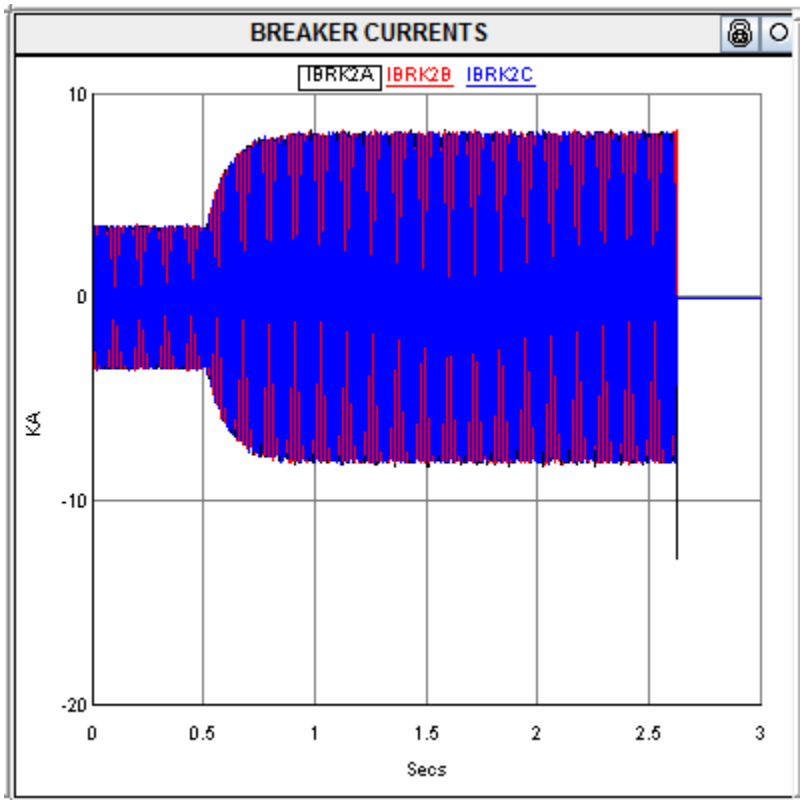

Figure 5.15. Breaker Currents during Over-voltage Simulation.

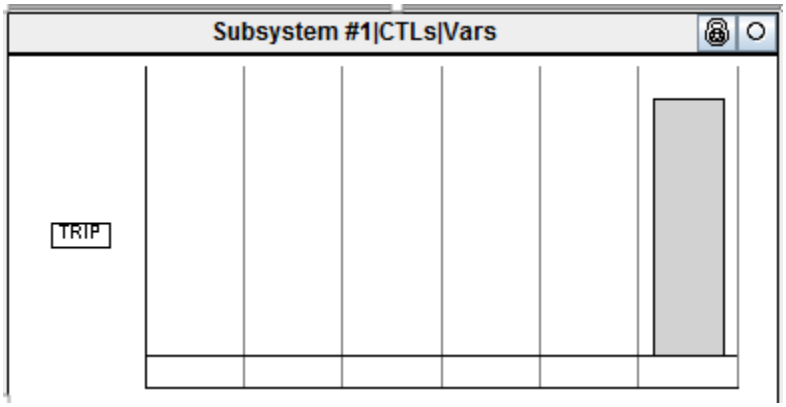

Figure 5.16. Trip signal.

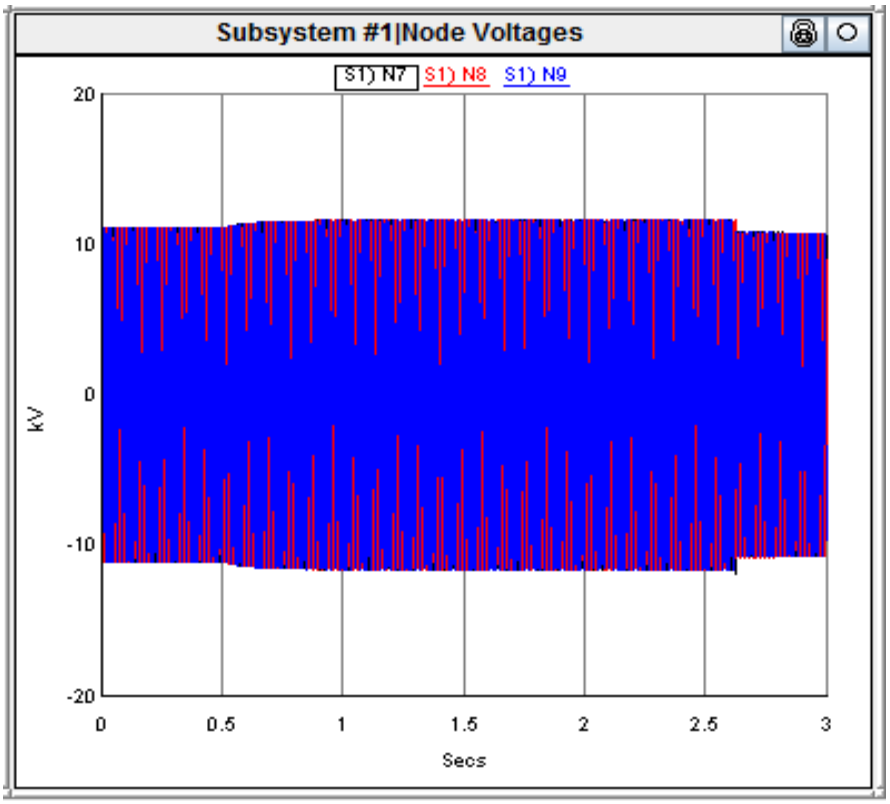

Figure 5.17. Bus Voltage at the Source.

The source voltage increases above the nominal value after 0.5 seconds and is stays above the nominal value for 2 seconds corresponding to 120 cycles, this condition triggers an over-voltage pick-up by the relay, after the specified time delay of 120 cycles elapses, the relay sends a trip signal shortly after 2.5 seconds and the trip occurs in real-time as can be observed in Figure 5.15. The burden voltages from the PT also shows that the voltage increases above nominal after 0.5 seconds and after 120 cycles, a trip occurs and the breaker is opened. The PT voltages ploted after 2.5 seconds when the breaker is opened represent noise.

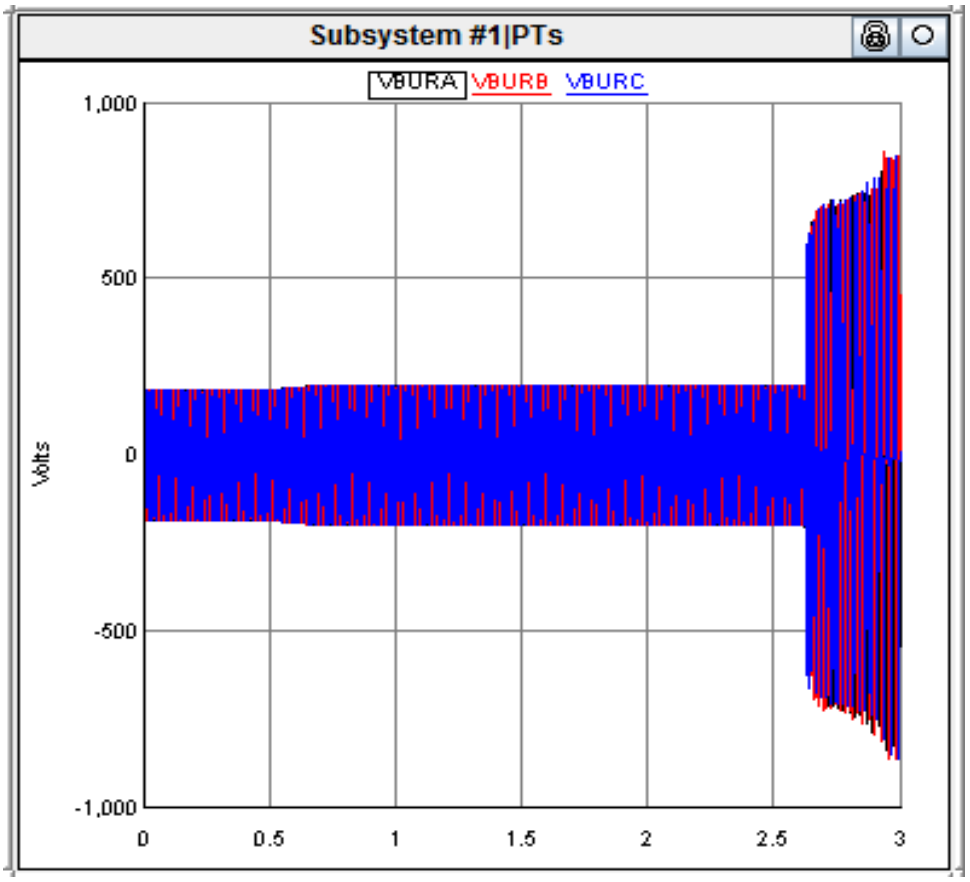

Figure 5.18. Burden Voltages at breaker.

The event recorded for the over voltage trip in the relay as shown in Figure 5.19 shows the later part of the simulation. From the current and voltage plots we can observe that the voltage values are above the nominal values from the start of the event record, and that the over-voltage element 1592P1T intitiates the trip signal that eventually the trips the breaker. It is also important to not that there is a short time delay between when the trip signal is initiatiated and when the relay actually opens up and the current goes to zero.

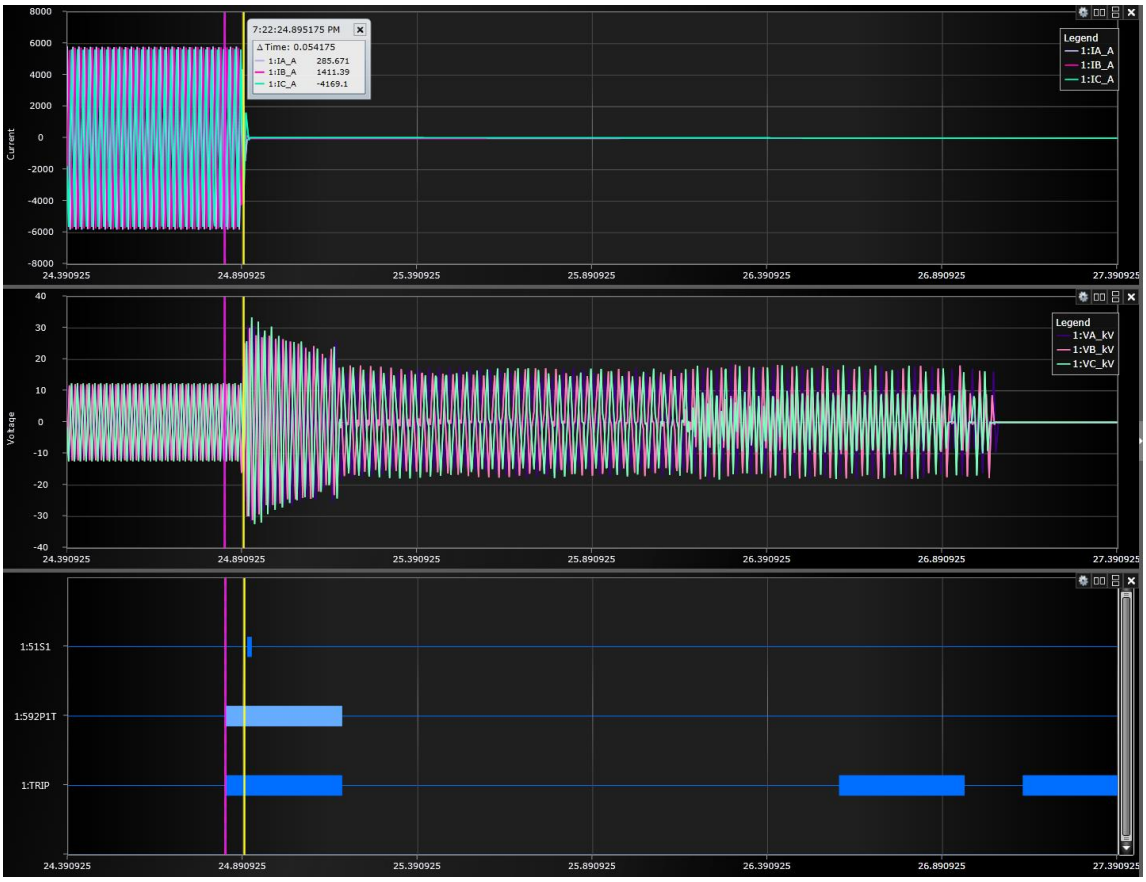

Figure 5.19. Synchrowave Event log of 59 Element trip.

5.5.4 Under Frequency Protection

In order to simulate an under frequency and over frequency disturbance, the frequency of the system is manually adjusted in the RTDS to initiate a trip event in the relay that is sent back into the RTDS. Figures 5.20-5.24 are measurements of the under-frequency simulation. According to Table 5.2, if an under frequency situation occurs, we expect a trip signal to be initiated within 0.5 seconds of the occurrence. To simulate an underfrequency in this case, the frequency dial of the system can be adjusted in real time as the simulation is running.

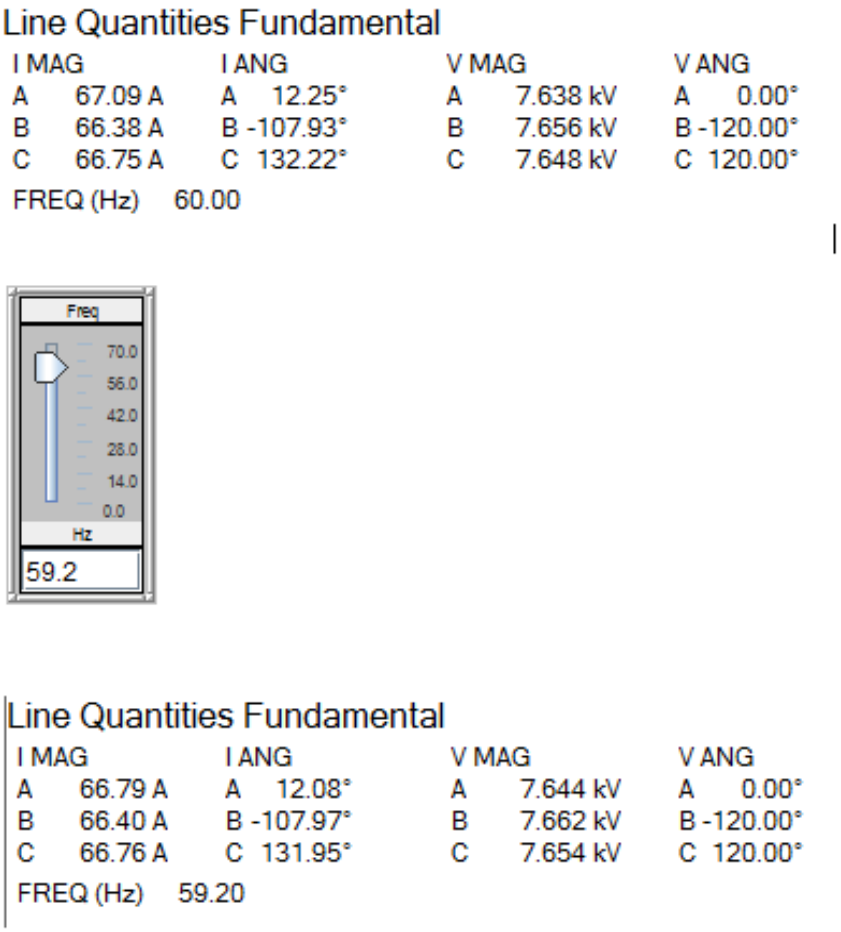

Figure 5.20. Adjustment of frequency in RTDS/Measurements in 421 HMI.

The relay settings are set to trip a the breaker for under-frequency occurrence within half of a second. Therefore as expected the above manual settings causes an under frequency to occur and a trip of the breaker as observed in Figure 5.21. The frequency is adjusted shortly after 0.5 seconds, and the trip ocurrs abiut half of a second later as can be observed in Figure 5.21. This indicates that the relay is sensitive to frequency deviations as small as 0.1Hz.

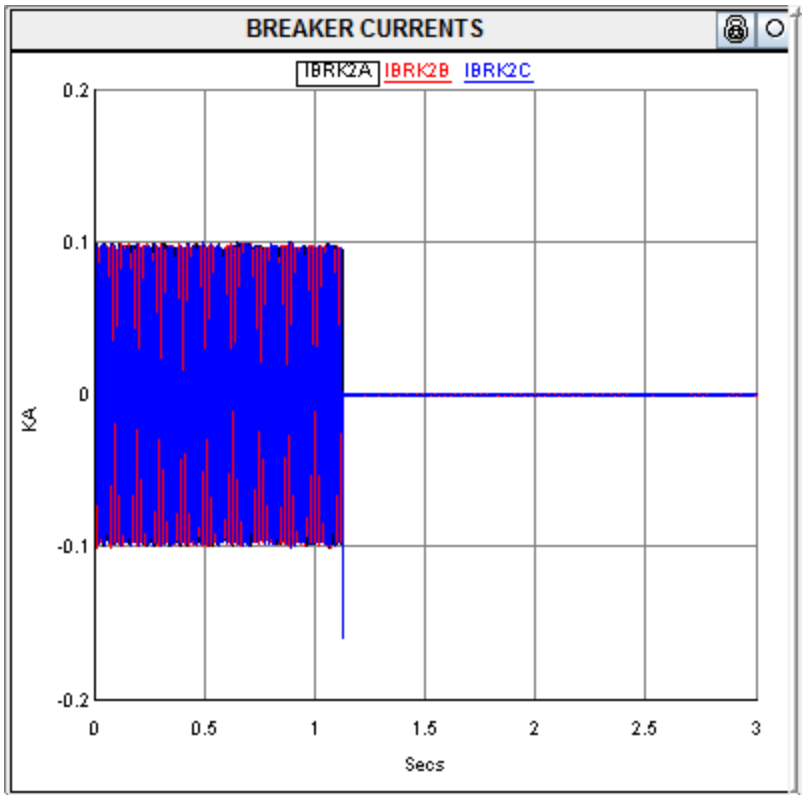

Figure 5.21. Breaker current measurements for under-frequency.

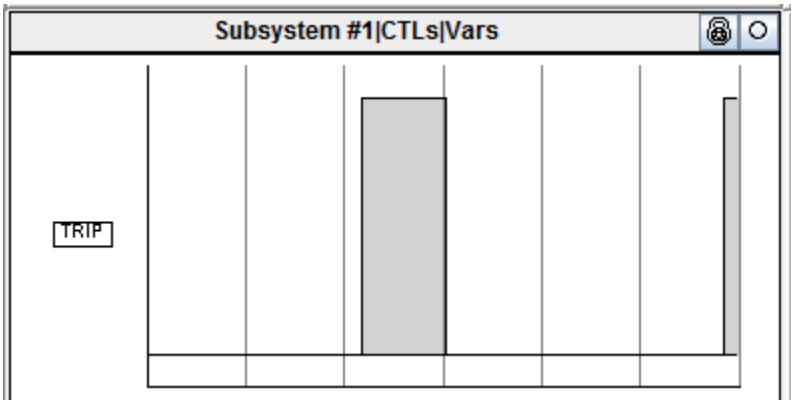

Figure 5.22. Trip signal Intiated to control breaker.

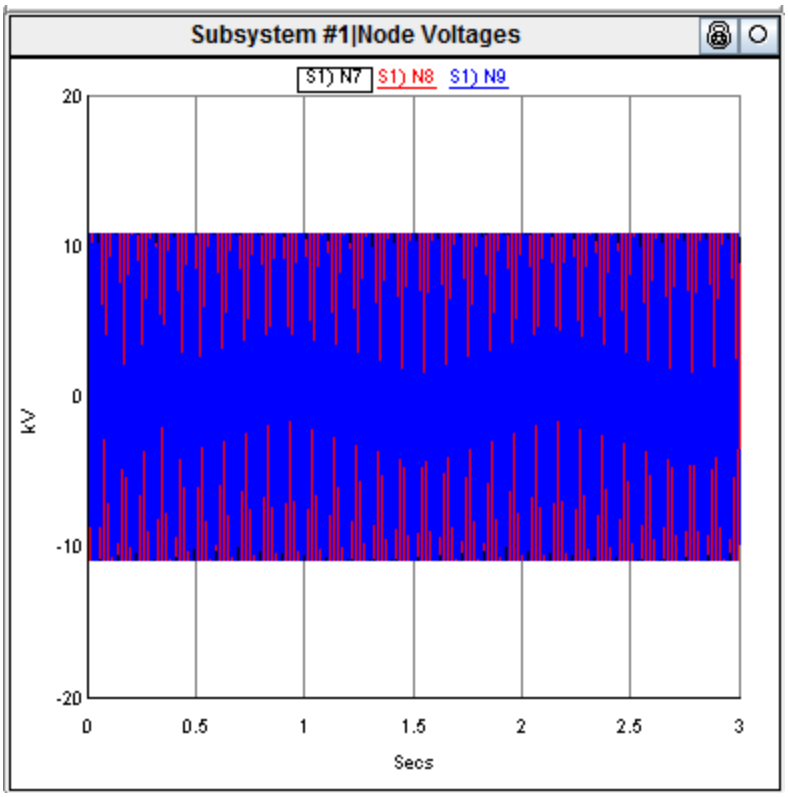

Figure 5.23. Voltage measurements showing frequency mismatch.

Observing the voltage plot above, we can see that after about 0.5 seconds, the frequency of the waveform changes, while the magnitude remains the same. Comparing voltage plots to the breaker current plots and the trip signal plots, we can observe that the trip signal occurs about 0.5 seconds after the frequency of the waveform changes, shortly after the 1 second marker. This indicates that the under frequency protection scheme is implemented.

In Figure 5.24, it can be observed that a trip signal is initiated by the under-frequency (81 element), corresponding to the relay settings as seen in Table 5.2.

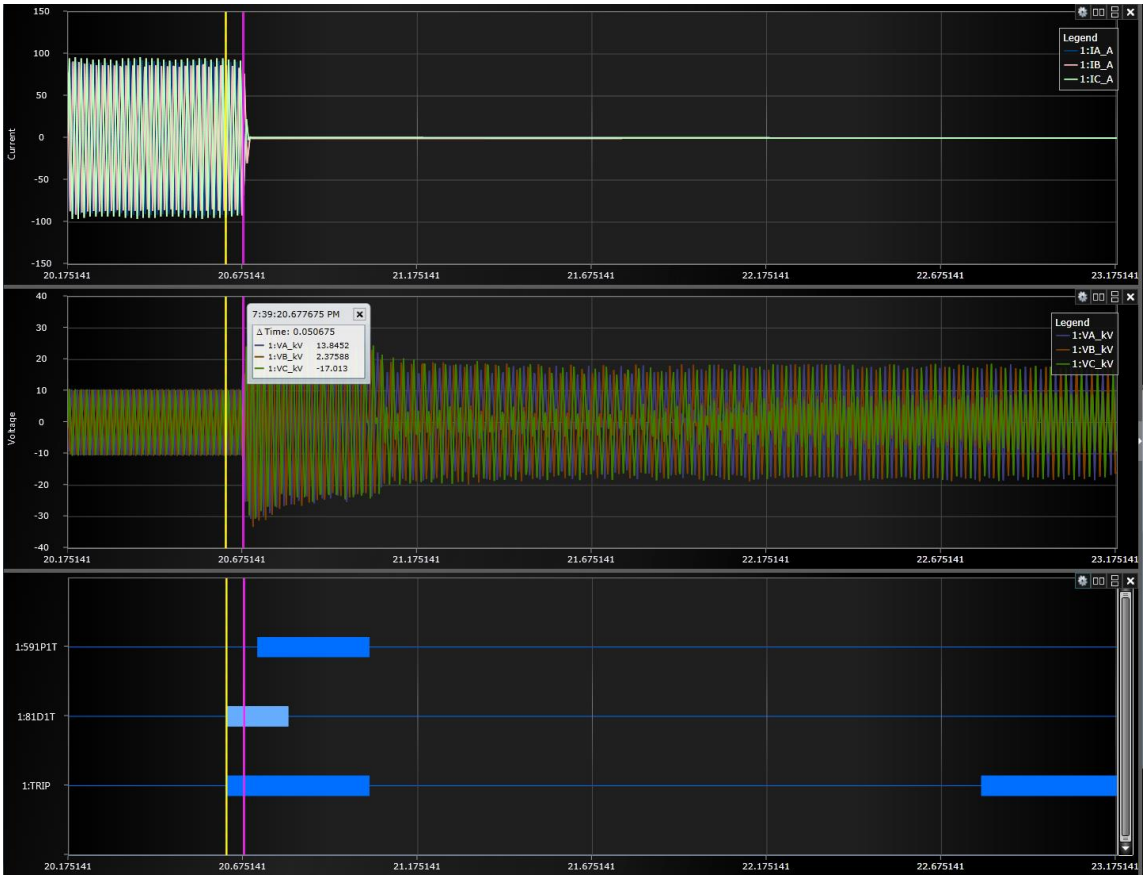

Figure 5.24. Under Frequency trip event.

CHAPTER SIX

Conclusion

The major contribution of this work was to present a concrete model for closed HIL simulation of a grid-connected PV system with protection hardware. The different components and systems that are comprised of the design of a grid-connected PV system and technical challenges that surround design and implementation of PV systems are highlighted and discussed in great detail. A grid-connected PV system is modeled and analyzed in a real time simulation environment, namely RTDS. The real time model is also interfaced with real protection hardware, to test the compatibility of the hardware and the reliability of the modeled system and controls.

In analyzing the PV system, we were able to establish that the system operation is dynamic and operates at stable conditions. The modeled system was also incorporated with protection hardware for extensive evaluation of the system performance. In the Hardware-in-loop tests, we were able to verify that the system operates under acceptable conditions during both steady-state operation and transient conditions.

The PV system controls were designed to output the maximum available power from the PV array to the grid through a DC to AC inverter, maintaining a reference AC voltage at the AC side of the inverter that was subject to the voltage of the grid side. This was achieved by implementing decoupled current controls and MPPT controls. At every time step, the MPPT algorithm determined the reference DC voltage that the PV system should operate on. This value is compared to the measured DC link voltage and the

difference is processed through PI control, to produce a power reference that controls the real power output at the inverter. The reactive power output is minimized by the controls to keep the power factor to as closs to unity as possible as can be observed in the power output anylysis of the PV system.

Under short transient conditions (< 10 cycles), the PV system controls are designed for the system to ride through certain fault conditions. However, for situations outside the contraints described in the IEEE 929-2000 standards, an accurate protection scheme was developed that protects the system from under/over voltage conditions, as well as under frequency conditions. The protection schemes was tested with a SEL-421 relay, and the protection schemes initiated tripping signals well within the standard constraints.

The advantages of simulating power systems in real time are vast, the ability to test the grid-connected PV system under real conditions as accomplished in this work, is a clear indication of various possibilities that exist in the real-time simulation environment. With the tools available in the RTDS, the real-time model developed can be further modified to accurately test the performance of grid-connected PV systems under various conditions.

Although we were able to test the system protection for various unstable conditions such as over/under voltage, over/under frequency, another important and mandatory protection scheme that requires extensive studying and analysis is anti-islanding control. Islanding of the grid occurs when the an inverter based system is disconnected from the primary grid but is still able to energize a local load. This situation is often referred to as an unintentional island, this is common with large PV systems which are connected to a substation feeder. In the case where an unintentional island occurs, this could pose a serious risk to maintenance personnel [17] as well as utuility equipment. It is therefore imperative

that islanding situations be extensively modeled, analyzed and studied, and anti-islanding protection schemes be developed to prevent the occurrence of an island.

BIBLIOGRAPHY

[1] International Energy Agency, *PVPS Report Snapshot of Global PV 1992-2-13*, Photovoltaic Power Systems Programme, Rep. 2014.

[2] S. Grover, *Energy, Economic, and Environmental Benefits of the Solar America Initiative,* NREL, Portland, OR, Tech. Rep., Aug. 2007.

[3] R. Lasserter, A. Akhil, C. Marnay, J. Stevens, J. Dagle, R. Guttromson, A.S. Meliopoulous, R. Yinger, and J. Eto, *Integration of Distributed Energy Resources, The CERTS Microgrid Concept,* U.S. Department of Energy, Rep., April, 2002.

[4] *IEEE Standard for Interconnecting Distributed Resources with Electric Power Systems*, IEEE Std 1547-2003, pp. 5,8 , July 28, 2003.

[5] *IEEE Recommended Practice for Utility Interface of Photovoltaic (PV) Systems*, IEEE Std 929-2000, pp. 4-6, Jan 30, 2000.

[6] A. A. Elbaset, M. S. Hassan, and H. Ali, "Performance analysis of grid-connected PV system," *2016 Eighteenth International Middle East Power Systems Conference (MEPCON)*, Cairo, 2016, pp. 675-682.

[7] N. Khaldi, H. Mahmoudi, M. Zazi, and Y. Barradi, "The MPPT control of PV system by using neural networks based on Newton Raphson method," *2014 International Renewable and Sustainable Energy Conference (IRSEC),* Ouarzazate, 2014, pp. 19-24.

[8] Ze Cheng, Hang Zhou, and Hongzhi Yang, "Research on MPPT control of PV system based on PSO algorithm," *2010 Chinese Control and Decision Conference*, Xuzhou, 2010, pp. 887-892.

[9] Y. Ba-khuraisa, A. Al-Hasani, I. Elshafiey, A. F. Sheta, and M. F. A. Aboud, "Experimental implementation of MPPT for PV systems," *2016 5th International Conference on Electronic Devices, Systems and Applications (ICEDSA),* Ras Al Khaimah, 2016, pp. 1-4.

[10] J. Ghaisari, M. Habibi, and A. Bakhshai, "An MPPT Controller Design for Photovoltaic (PV) Systems Based on the Optimal Voltage Factor Tracking," *2007 IEEE Canada Electrical Power Conference*, Montreal, Que., 2007, pp. 359-362.

[11] K. J. George, "Direct control method applied for improved incremental conductance mppt using SEPIC converter," *2014 International Conference on Green Computing Communication and Electrical Engineering (ICGCCEE)*, Coimbatore, 2014, pp. 1-6.

[12] S. Jianping and L. Xiaozheng, "A new MPPT control strategy: Study of auto-adapted step size incremental conductance method based on segmented numerical approximation," *2011 International Conference on Mechatronic Science, Electric Engineering and Computer (MEC)*, Jilin, 2011, pp. 239-242.

[13] C. Natesan, A. Devendiran, S. Chozhavendhan, D. Thaniga, and R. Revathi, "IGBT and MOSFET: A comparative study of power electronics inverter topology in distributed generation," *2015 International Conference on Circuits, Power and Computing Technologies [ICCPCT-2015]*, Nagercoil, India.

[14] R. Technologies, "Vsc small time step modeling," *RTDS Manuals and Documentation*, Winnipeg, 2009.

[15] L. Xu, *Modeling, Analysis and Control of Voltage-Source Converter in Microgrids and HVDC,* Ph.D dissertation, Dept. Electrical Engineering, College of Engineering, Univ of South Florida, U.S, 2013.

[16] Y. Amirnaser, *Voltage - sourced converters in power systems: modeling, control, and applications*, 1st ed. New Jersey: IEEE Press, 2012.

[17] S. Kim, J. Jeon, C. Cho, E. Kim, and J. Ahn, "Modeling and simulation of a grid-connected PV generation system for electromagnetic transient analysis," *Solar Energy*, vol. 83, no. 5, pp. 664-678, 2009.

[18] M. Abdel-Salam, R. Kamel, M. Khalaf, and K. Sayed, "Analysis of overcurrent numerical-relays for protection of a stand-alone PV system," *2014 Saudi Arabia Smart Grid Conference (SASG)*, Jeddah, 2014, pp. 1-6.

[19] C. C. Yeh, C. S. Chen, T. T. Ku, C. H. Lin, C. T. Hsu, Y. R. Chang, and Y. D. Lee, "Design of Special Protection System for an Offshore Island with High PV Penetration," *2016 IEEE/IAS 52nd Industrial and Commercial Power Systems Technical Conference (I&CPS)*, Detroit, MI, 2016, pp. 1-7.

[20] R. Varier and N. M. Pindoriya, "A novel active anti-islanding protection scheme for grid-interactive roof-top solar PV system," *2014 Eighteenth National Power Systems Conference (NPSC)*, Guwahati, 2014, pp. 1-6.

[21] V. John, Zhihong Ye, and A. Kolwalkar, "Investigation of anti-islanding protection of power converter based distributed generators using frequency domain analysis," *IEEE Transactions on Power Electronics*, vol. 19, no. 5, pp. 1177-1183, Sept. 2004.

[22] O. Nzimako and R. Wierckx, "Modeling and Simulation of a Grid-Integrated Photovoltaic System Using a Real-Time Digital Simulator," *2016 IEEE Transactions on Industry Applications.*

[23] [Online]. Available: https://www.rtds.com/

[24] N. Watson and A. Farzanehrafat, "Three-phase transient state estimation algorithm for distribution systems," *IET Generation, Transmission & Distribution*, vol. 8, no. 10, pp. 1656-1666, 2014.

[25] R. Technologies, *RTDS Manuals and Documentation*, Winnipeg, 2009.

[26] R. Technologies, "Modeling Renewable and DG's in RTDS,"*RTDS Manuals and Documentation*, Winnipeg, 2009.

[27] [Online]. Available: http://www.samlexsolar.com/learning-center/solar-cell-module-array.aspx.

[28] D. S. Chan and J. C. Phang, "Analytical Methods for the Extraction of Solar-Cell Single-and Double-Diode Model Parameters from I-V Characteristics," *IEEE Transactions on Electronic Devices*, vol. 34, no. 2, pp. 286-293, Febuary 1987.

[29] A. Yazdani and R. Iravani, *Voltage-Sourced Converters in Power Systems: Modeling, Control, and Applications*, New Jersey: Wiley-IEEE Press, 2010.

[30] R. Technologies, "Vsc small time step tutorial,"*RTDS Manuals and Documentation*, Winnipeg, 2009.

[31] O. Nzimako, *Real Time Simulation of a Microgrid with Distributed Energy Resources*, M.S. thesis, Dept. Elect and Comp Eng., Univ of Manitoba, Winnipeg, Canada, 2015.

[32] Schweitzer Engineering Laboratories, *SEL-421 Relay, Protection And Automation System, Instruction Manual.*